JEM Journal of Experimental Medicine

ARTICLE

Rab5 improves CAR T cell efficacy via reducing fratricide and maintaining surface CAR levels

Meidi Gu[1,2], Kaitlin A. Read[1,2], Vipin Bhardwaj[1,2], Edmund J. Carvalho[1,2], David Nardo[1,2], Justin C. Shayne[1,2], Divanshu Shukla[1,2], Wei Liu[2,3], Donald L. Siegel[2,3], Neil C. Sheppard[2,3], Michael C. Milone[2,3], Adam D. Cohen[4], Alfred L. Garfall[4], and James L. Riley[1,2]

We show continuous tumor exposure results in a loss of chimeric antigen receptor (CAR) T cell (CART) endocytic activity due to downregulation of Rab5. Loss of endocytic activity exacerbates the effects of trogocytosis, the bidirectional transfer of tumor target antigens and CARs between malignant cells and CARTs, resulting in CART dysfunction and fratricide. Constitutive expression of Rab5 within the CARTs reduced fratricide by reducing the amount of trogocytosed antigens on the cell surface, while simultaneously enhancing CAR availability through dissociation of CAR from target, recycling unbound CAR back to the plasma membrane, and limiting CAR capture by tumor cells. Rab5-expressing CARTs exhibited superior antitumor activity in both BCMA-CARTs isolated from the bone marrow of treated patients and mesothelin-specific CARTs in a solid tumor model. These studies uncover an unexpected relationship between endocytosis and CART function and suggest that pairing Rab5 with CAR expression could improve the clinical efficacy of CART therapy.

Introduction

Chimeric antigen receptor (CAR) T cell (CART) therapy has led to remarkable therapeutic responses in patients with certain hematological malignancies (Cappell and Kochenderfer, 2023), yet its efficacy in solid tumors remains limited (June et al., 2018; Rafiq et al., 2020). Significant effort has been devoted to boosting the efficacy of CARTs to expand the number of patients who could benefit from this therapy, including providing signals that prolong CART persistence (Chan et al., 2024; Doan et al., 2024; Kagoya et al., 2018; Shum et al., 2017), resist T cell exhaustion (Lynn et al., 2019), and help CARTs overcome the immunosuppressive tumor microenvironment (Narayan et al., 2022). While the molecular mechanisms underlying CART dysfunction in solid tumors are not fully understood, this knowledge is critical to develop rational approaches aimed at improving broad CART function.

In the tumor microenvironment, direct cell–cell contact is a primary trigger for reprogramming T cell antitumor functions (Kim et al., 2024). Trogocytosis is a dynamic form of membrane trafficking between 2 cells, with important roles in immune cell interactions and tumor biology (Kim et al., 2025; Rechavi et al., 2009). For CARTs, trogocytosis has been shown to be detrimental to function, as the transfer of tumor antigens to CARTs can trigger fratricide and immune dysfunction (Hamieh et al., 2019), while CAR molecules transferred into tumor cells impair antigen recognition and cytotoxicity (Zhai et al., 2023). Trogocytosis can be considered a variant of phagocytosis or transendocytosis (Rechavi et al., 2009). Attempts to limit both processes have been used to increase CAR surface expression (Xu et al., 2024; Zhou et al., 2023). Interestingly, studies indicate that the endocytic-recycling pathway is crucial for sustaining CAR surface expression and functional durability (Li et al., 2020; Xie et al., 2025), suggesting that simply blocking endocytosis may be counterproductive. These observations suggest that a deeper understanding of how trogocytosis is regulated and how it affects CARTs, particularly in the context of tumor–CART interactions is needed.

Endocytosis plays a key role in maintaining membrane health, signal transduction, lipid homeostasis, and mitosis, but how its activity affects CARTs is limited (Charpentier and King, 2021; Delgoffe et al., 2021). Rab GTPase family proteins are central organizers of membrane trafficking (Behnia and Munro, 2005; Homma et al., 2021; Zerial and McBride, 2001) and play essential roles in processes ranging from early endocytosis to lysosomal degradation (Birgisdottir and Johansen, 2020; Soreng et al., 2018; Zhen and Stenmark, 2015). The human genome encodes >60 Rab GTPases. Among them, Rab5, an early endosome marker, plays a crucial role in the internalization and trafficking of membrane receptors, including TCRs (Bucci et al.,

[1]Department of Microbiology, University of Pennsylvania, Perelman School of Medicine, Philadelphia, PA, USA; [2]Center for Cellular Immunotherapies, University of Pennsylvania, Perelman School of Medicine, Philadelphia, PA, USA; [3]Department of Pathology and Laboratory Medicine, University of Pennsylvania, Perelman School of Medicine, Philadelphia, PA, USA; [4]Division of Hematology-Oncology, Department of Medicine, University of Pennsylvania, Perelman School of Medicine, Philadelphia, PA, USA.

Correspondence to James L. Riley: rileyj@upenn.edu; Meidi Gu: meidi.gu@pennmedicine.upenn.edu.

1992; Yuan and Song, 2020; Zerial and McBride, 2001). Mutations in the Rab5 gene directly affect TCR transport and downstream TCR signaling (Andre et al., 1997; Finetti et al., 2014; Redpath et al., 2019). Here, we show that continuous tumor engagement results in Rab5 downregulation, which is associated with the loss of endocytic activity and CART function. This impaired endocytic activity amplifies the detrimental effects of trogocytosis on CART function by allowing target antigen accumulation on T cell surfaces and promoting CAR capture by tumors. Introduction of Rab5 into CARTs demonstrated superior target antigen clearance, preserved CAR surface expression, and improved antitumor efficacy both *in vitro* and *in vivo*. These findings uncover that loss of endocytic activity is a previously unrecognized mechanism of CART dysfunction and highlight membrane trafficking reprogramming as a promising strategy to augment CART therapy.

Results

Continuous tumor interactions lead to downregulation of endocytic activity in CARTs

Long-term interactions with tumors limit CART function, which can result in tumor relapse (Delgoffe et al., 2021). A continuous antigen exposure (CAE) assay models this process *in vitro* and mimics key features of CART dysfunction found in patients lacking durable CART responses (Good et al., 2021). We adapted this assay to study CART dysfunction using CD19-specific CARTs that employed 4-1BB and CD3 zeta signaling domains (19BBz) and challenged them with K562 cells expressing CD19 and GFP (K.19.GFP) every 2 days to better understand how this dysfunction occurs (Fig. S1 a). Consistent with previous findings, CARTs initially controlled tumor growth, but eventually lost this capacity. Moreover, the number of CARTs diminished over time, which could reflect tumor outgrowth or CART elimination (Fig. 1 a).

To better understand the mechanisms underlying this dysfunction, we used bulk RNA sequencing (RNA-seq) to compare CARTs before CAE (day 9 after T cell stimulation) with CARTs after three rounds of tumor stimulation in the CAE assay (third-CAE). Gene expression was significantly altered and samples segregated into distinct clusters by tumor stimulation condition, suggesting major phenotypic changes (Fig. S1, b and c). Many of the observed changes in gene expression reflected the fact that CAE-CARTs were more activated than those that had rested down after 9 days of culture (Fig. S1 d). Unexpectedly, bulk RNA-seq analysis revealed that multiple genes associated with endocytosis (GO:0030100) were downregulated in CAE-CARTs (Fig. 1, b and c). This was surprising given that our studies and others have shown that activated T cells exhibit higher endocytic activity than resting T cells (Charpentier et al., 2020; Rossatti et al., 2022) (Fig. S1 e). To determine whether continuous tumor exposure altered endocytic function in CARTs, we incubated resting CARTs and CAE-CARTs with AM1-44, a dye widely used to track and visualize cell membrane activity, particularly endocytosis (Sara et al., 2005). CAE-CARTs exhibited markedly reduced dye uptake compared with unchallenged CARTs (Fig. S1, f and g). Using pHrodo dextran, which is specifically internalized through endocytosis, we again observed impaired uptake in CAE-CARTs (Fig. 1, d and e), validating that CAE results in the loss of endocytic activity in T cells. More importantly, to test whether tumor antigen exposure directly impairs endocytosis *in vivo*, we co-infused anti-CD19 (19BBz) and anti-mesothelin (MESOBBz) CARTs into mice bearing CD19-expressing tumors. After 14 days, the endocytic activity of these two tumor-infiltrating CART populations was analyzed, and 19BBz CARTs displayed markedly reduced endocytic activity relative to the MESOBBz CARTs (Fig.1, f and g), indicating that tumor engagement suppressed T cell endocytic activity. Among the Rab family proteins that are downregulated by tumors (Fig.1 c), Rab5 is the central regulator of early endosomes and overall endocytic activity (Grbovic et al., 2003; Yuan and Song, 2020). It is poorly expressed in resting T cells, induced upon T cell activation, and wanes as CARTs return to quiescent state (Fig. S1 h). Importantly, upon continuous tumor interaction, Rab5 expression in CARTs was markedly downregulated, despite a transient initial increase (Fig. 1 h). Thus, reduction in Rab5 expression correlates with loss of endocytic activity in CARTs following tumor engagement. Together, these results indicate that continuous tumor interactions lead to a loss of endocytic activity within CARTs, which correlates with impaired CART function.

Forced Rab5 expression restores endocytic activity and CART function

To test whether restoring Rab5 expression could rescue endocytic activity in CARTs, we co-expressed Rab5 together with 19BBz CAR using a T2A sequence (19BBz-Rab5, or Rab5-CART in reference to all Rab5 overexpression constructs) (Fig. S2 a). We also co-expressed Rab4 and Rab11, which are Rab family members involved in endocytic recycling and exocytosis (Longatti et al., 2012; Ward et al., 2005). In contrast to control (tEGFR), Rab4, and Rab11-expressing CARTs, Rab5-expressing CARTs were able to uptake both the pHrodo dextran and AM1-44 dye throughout CAE (Fig. 2, a and b), indicating endocytic activity was maintained throughout continual tumor engagement when CARTs were able to maintain Rab5 expression. Next, we asked if restoration of endocytic activity resulted in improved CART activity within the CAE assay. Strikingly, Rab5-CARTs exhibited prolonged tumor-killing capacity compared with controls, Rab4, or Rab11-CARTs (Fig. 2, c and d) and maintained sustained Rab5 expression during the CAE assay (Fig. S2 b). Rab5 is known to interact with multiple signaling molecules, including PI3K family members that could potentially influence CART survival or function (Yuan and Song, 2020). However, transcriptional profiling of Rab5-CARTs in the presence or absence of tumors revealed only modest differences relative to the control CARTs (Fig. S2, c and d), suggesting that Rab5 alone is sufficient for improved endocytic activity in CARTs. Moreover, surface expression of key T cell markers (TCR, CD25, CD28, and CD45) and checkpoint markers (PD-1, Tim-3, and Lag-3) were unaltered by enforced Rab5 expression during CAE assay (Fig. S2, e and f). These results suggest that enhanced endocytic and cytolytic activity of Rab5-CARTs is directly attributable to Rab5 itself, rather than indirect effects on T cell activation or phenotype. Given that Rab5's GTPase activity functions as an on/off switch for its regulation of endocytosis (Homma et al., 2021; Wang et al., 2024), we next tested whether this activity is

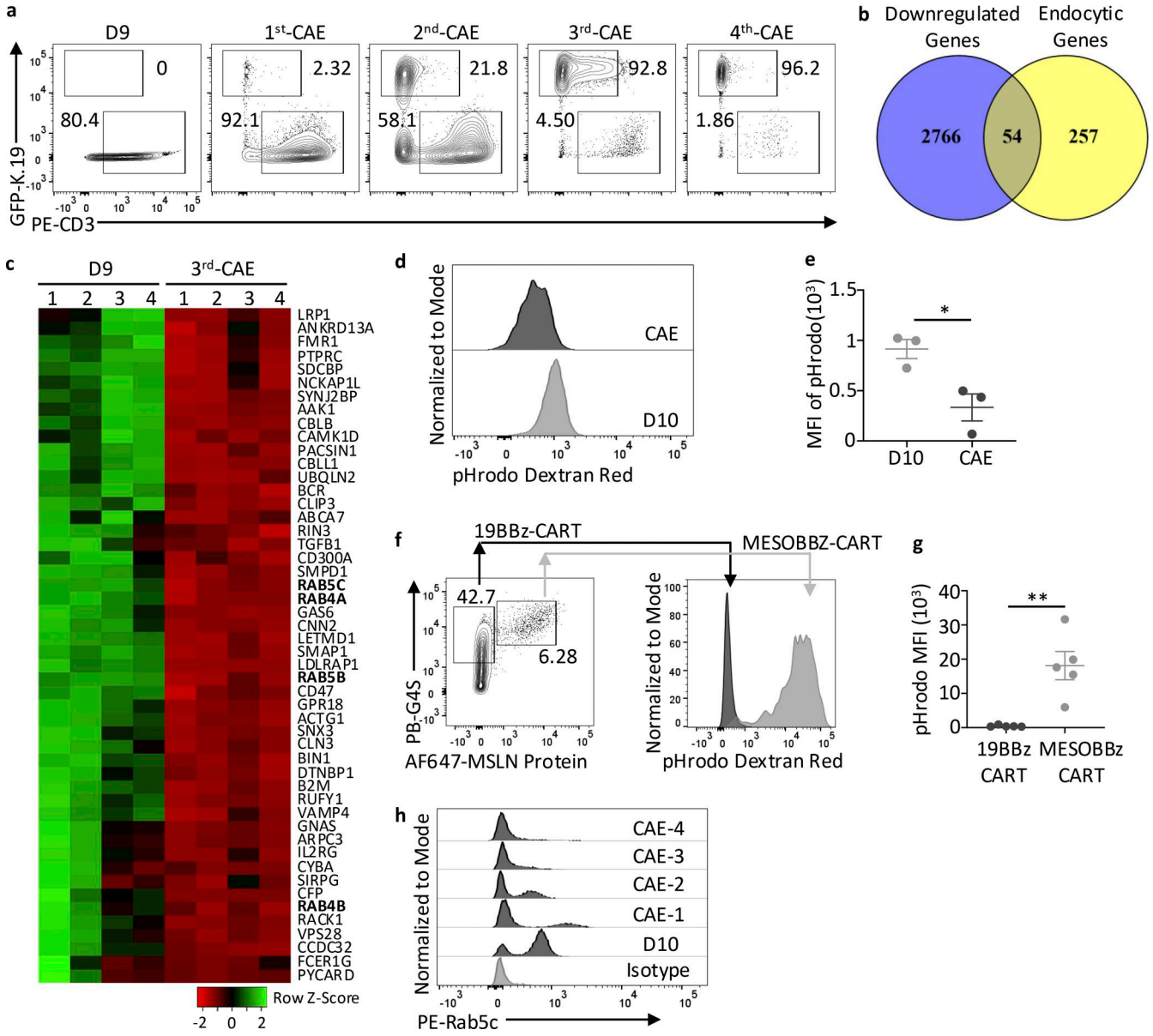

Figure 1. **Continuous tumor interactions lead to downregulation of endocytic activity in CARTs. (a)** Flow cytometry of the CAE assay at indicated time points, used to analyze the presence of K.19 tumor cells (GFP⁺) and 19BBz-tEGFR CARTs (CD3⁺). Primary human T cells were activated and transduced with 19BBz-CAR. After 9 days of culture, 1 × 10^6 CAR-positive T cells were co-cultured with 2 × 10^6 K562 cells expressing CD19 and GFP (K.19.GFP). Every 2 days, additional 2 × 10^6 K.19.GFP were added to the co-culture assay. Data are representative of three independent experiments with samples from unique healthy donors. **(b)** Venn diagram showing the overlap between downregulated genes and genes associated with endocytic processes. Bulk RNA-seq identified over 2,000 genes downregulated in 19BBz-tEGFR CARTs after tumor engagement, of which 54 were annotated as endocytosis-related. **(c)** Heatmap showing bulk RNA-seq expression profiles of endocytosis-related genes in b, excluding four genes with low read counts. Each column represents an individual donor sample (n = 4 healthy donors). **(d and e)** Endocytic activity of CARTs obtained on day 10 after T cell stimulation or after a second-round CAE assay was measured by uptake of pHrodo Red dextran at 37°C for 20 min, analyzed by flow cytometry. Data are representative of three independent experiments with samples from unique healthy donors. **(f and g)** pHrodo Red dextran endocytosis was assessed in tumor-infiltrating CARTs. 19BBz-tEGFR and MESOBBz-tEGFR CARTs were mixed at a 1:1 ratio and infused into K.19.GFP tumor-bearing mice 7 days after tumor implantation. 14 days after CART infusion, tumor-infiltrating CARTs were isolated and incubated with pHrodo Red dextran at 37°C for 20 min. Endocytic activity was compared between CD19-responsive 19BBz-tEGFR and CD19-nonresponsive MESOBBz-tEGFR CARTs. Data are representative of two independent experiments, n = 5 mice for each group. **(h)** Intracellular Rab5 expression level in 19BBz-tEGFR CARTs, measured during the CAE assay by flow cytometry; data are representative of two independent experiments with samples from unique healthy donors. Error bars show mean ± SEM. Statistical comparisons were made using unpaired t tests. *P < 0.05 and **P < 0.01.

required to maintain CART function. We generated a GTPase-defective Rab5 mutant (S35N) and assessed its effect in the CAE assay. The S35N variant acted as a dominant-negative mutant, causing CARTs to exhibit significantly impaired tumor-killing activity (Fig. 2, e–g). Collectively, these findings demonstrate that introducing a properly regulated Rab5 restores CART endocytic activity during continuous tumor challenge, thereby rescuing their capacity to become serial killers.

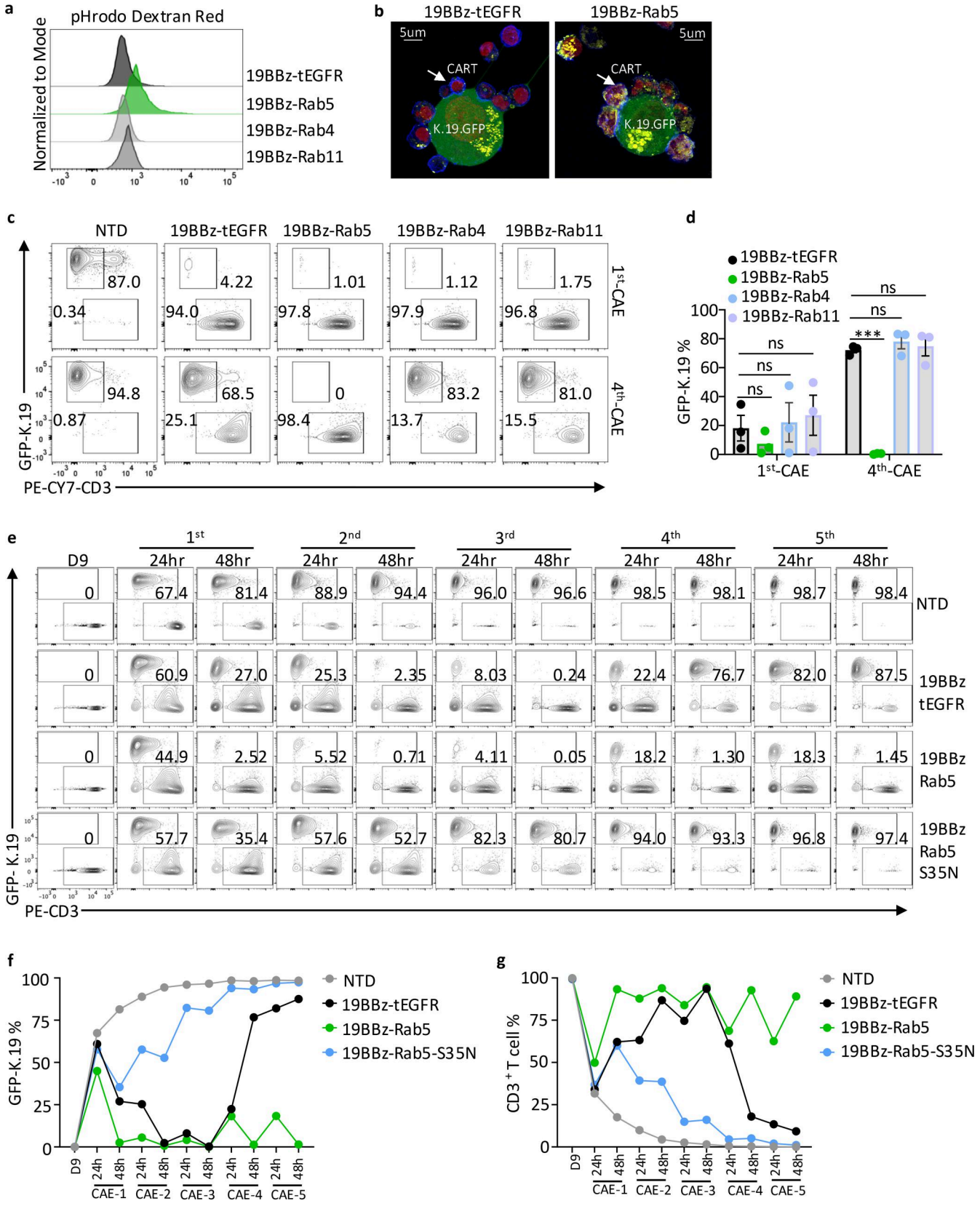

Figure 2. **Forced Rab5 expression restores endocytic activity and CART function. (a)** pHrodo Red dextran endocytosis in 19BBz CARTs expressing tEGFR, Rab5, Rab4, or Rab11 from third round CAE assay, measured by flow cytometry. Data are representative of three independent experiments with samples from unique healthy donors. **(b)** Comparison of endocytosis activity between tEGFR-CARTs and Rab5-CARTs by tracking AM1-44 uptake in the presence of K.19.GFP using confocal microscopy. GFP (green), CD45 (blue), nuclei (red), and AM1-44 (yellow) are shown. Data are representative of two independent experiments.

(c and d) Representative flow cytometry plots of K.19.GFP tumor cell killing by 19BBz-tEGFR, -Rab5, -Rab4, or -Rab11 CARTs in CAE assay (c). Summary data of K.19.GFP survival during CAE assay time points shown in c. Each dot represents an independent experiment using a unique donor (d). Data are representative of three independent experiments with samples from unique healthy donors. **(e)** Representative flow cytometry plots of K.19.GFP tumor cells after being mixed with NTDs, tEGFR-CARTs, Rab5-CARTs, or Rab5-S35N-CARTs at indicated time points in the CAE assay. **(f and g)** Summary of K.19.GFP tumor cells remaining (f) and CD3$^+$ T cell persistence (g) during the indicated CAE assay, as shown in e. Experiments shown in e–g are representative of three independent experiments with samples from independent healthy donors. Error bars show mean ± SEM. Statistical comparisons were made using unpaired *t* tests. ***P < 0.001; ns, not significant.

Rab5 expression facilitates target antigen clearance and resistance to fratricide

Since endocytosis plays a key role in cell membrane homeostasis by recycling proteins on/off the cell surface, we asked if loss of endocytic activity in CAE-CARTs would directly lead to the accumulation of tumor-derived proteins, such as CD19, by trogocytosis. Control CARTs maintained high levels of CD19 on their cell surface throughout the CAE assay, whereas CARTs expressing Rab5 had negligible levels of surface CD19 (Fig. 3, a and b). However, at early time points of the co-culture, CD19 acquisition was comparable between control and Rab5-CARTs (Fig. S2 g), suggesting that Rab5 was not influencing the capture of antigen but rather its clearance from the cell surface. CD19 presence on T cells could reflect CAR-binding CD19 or trogocytosis of tumor antigens. To distinguish between these two possibilities, we used two CD19-specific antibodies: FMC63, which was the antibody used to make scFv domain of the CD19 CAR (Milone et al., 2009) and whose binding should be blocked if the CD19 is bound by the CAR, and HIB19, whose binding to CD19 is unaffected by CAR engagement. We observed two populations: one in which CD19 was accessible to both antibodies, indicating trogocytosed antigen; the other in which CD19 was recognized only by HIB19, representing CD19 that was bound by CARs. Rab5-CARTs had a lower proportion of double positive CD19 populations, indicating reduced trogocytosis (Fig. 3 c). We hypothesized that this reduction of trogocytosed antigen would make Rab5-CARTs less susceptible to fratricide. To test this, we incubated control or Rab5 CARTs expressing mCherry (19BBz-mCherry-T2A-tEGFR or -Rab5, shortened to mCherry-Rab5) with K.19.GFP cells for 1 day to allow CD19 acquisition (Fig. 3, d and e). These mCherry-CARTs were then mixed with 19BBz-BFP-T2A-tEGFR CARTs to distinguish the fresh CARTs from those that may have trogocytosed CD19 (Fig. 3, d and f). After 2 days of co-culture, mCherry-Rab5 CARTs were abundant, whereas mCherry-tEGFR CARTs were largely depleted, and only CAR-dim cells survived (Fig. 3, f–h). Likewise, significantly fewer apoptotic cells were detected in mCherry-Rab5 CARTs relative to control (Fig. 3, i and j), indicating Rab5-CARTs are less susceptible to fratricide than control CARTs. Together, these results demonstrate that Rab5 expression promotes clearance of trogocytosed antigens and reduces CART fratricide, thereby sustaining CART function under chronic antigen exposure.

Rab5 expression enables recycling of unbound CARs back to the CART cell surface

The results above demonstrate that Rab5 expression reduces trogocytosed antigen-triggered fratricide. We were also interested in whether Rab5 could facilitate the clearance of CAR-bound CD19 from the cell surface. We first measured CAR availability during the CAE assay and observed that control CARTs lost their ability to bind CD19 by the third tumor challenge, whereas Rab5 CARTs maintained it throughout the CAE assay (Fig. 4, a and b; and Fig. S3, a–d). Similar data were obtained in CARTs containing a CD28ζ signaling domain, indicating that this process is not dependent upon the costimulation domain (Fig. S3, e–h). Next, we asked how Rab5-mediated endocytosis regulates the fate of CAR–CD19 complexes. During endocytosis, the early endosome is the initial destination of surface receptor trafficking (Andre et al., 1997; Hayes et al., 2002). Thus, to determine whether Rab5 promotes CAR endocytosis, we purified early endosomes from mCherry-tagged control or Rab5-CARTs from the third round of the CAE assay. Endosomes from Rab5-CARTs contained mCherry, Rab5, CD3ζ, and a larger form of CD3ζ representing the CAR, whereas only endogenous CD3ζ was detected in control CARTs (Fig. 4 c). These results indicate that Rab5 promotes CAR internalization and retention in early endosomes. To determine whether CARs undergo endocytic recycling back to the cell surface, we added a FLAG tag juxtaposed to the membrane proximal region of the CAR, allowing CAR detection regardless of whether the CAR is bound to CD19. We stained these CARTs with anti-FLAG antibody and observed a population of FLAG positive, FMC63 idiotype negative CARTs, representing CARTs whose CARs are occupied by CD19. After 1 h, control CARTs still maintain a sizable population of FLAG$^+$FMC63$^-$CARTs, whereas this population was markedly reduced in Rab5-CARTs. This indicates that Rab5 promotes the clearance of CD19-bound CARs (FLAG$^+$ FMC63$^-$) and return of unbound CARs (FLAG$^+$ FMC63$^+$) back to the cell surface (Fig. S4 a; and Fig. 4, d and e). This pool of unbound CARs was even more pronounced during the CAE assay, where Rab5-CARTs maintained abundant unengaged surface CARs, whereas control CARTs were frequently occupied by CD19 (Fig. 4, f and g).

In these CAE studies, we also observed that Rab5 CARTs maintained higher surface CAR levels, as indicated by FLAG staining (Fig. 4 h). Since CD19 binding does not interfere with FLAG antibody recognition, this suggests that Rab5 helps CARTs maintain surface CAR persistence. Trogocytosis is a bidirectional transfer process in which CARs can be stripped from T cells and internalized into tumor cells (Zhai et al., 2023). By mixing mCherry-control CARTs with K.19.GFP tumors in a CAE assay, we also observed CAR capture by tumors (Fig. S4 b). Importantly, Rab5-CARTs co-cultured with tumor cells displayed markedly higher levels of CARs on their cell surface relative to control CARTs (Fig. 4, i and j). To further understand the fate of CAR after CARTs are co-cultured with tumors, we attached ascorbate peroxidase 2 (APEX2) to the CAR construct and visualized CAR subcellular localization by transmission electron

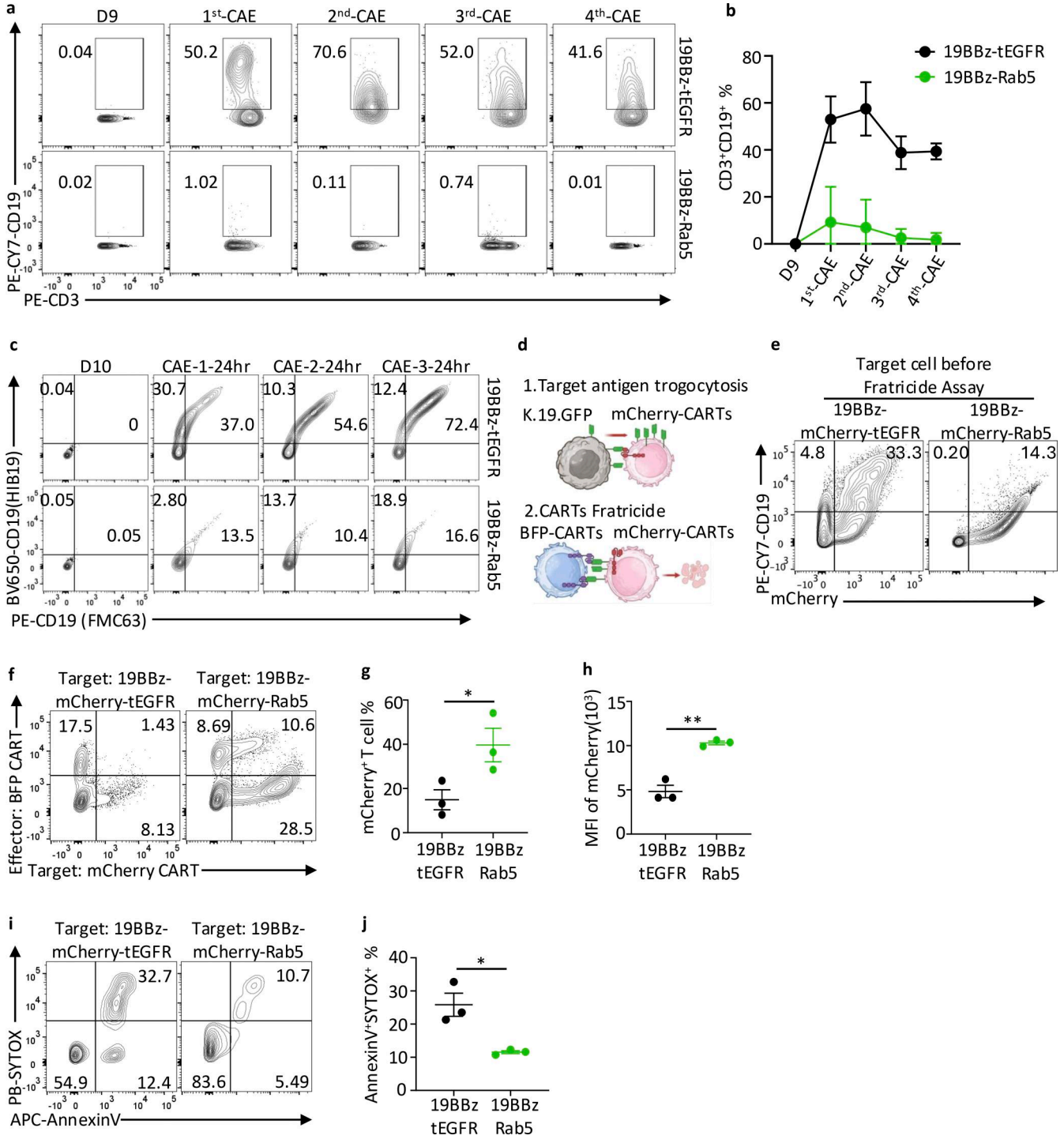

Figure 3. **Rab5 expression facilitates target antigen clearance and resistance to fratricide. (a)** Measurement of CD19 on the surface of control or Rab5-CARTs was measured by flow cytometry at indicated time points during the CAE assay. **(b)** Summary data of a. Data are representative of three independent experiments with samples from unique healthy donors. **(c)** Representative flow cytometry plots of CD19 on T cell surface, measured at the indicated CAE assay time points using anti-CD19 (HIB19) and anti-CD19 (FMC63) antibodies. Data are representative of three independent experiments. **(d)** Schematic representation of the CART fratricide assay used in e–j. mCherry-fused 19BBz-CARTs acquired the CD19 antigen from K.19.GFP tumor cells, triggering fratricide mediated by BFP-fused 19BBz-CARTs. **(e)** Representative flow cytometry plots of mCherry-positive tEGFR or Rab5 CARTs 24 h after co-culture with K.19.GFP cells, measuring surface CD19 and mCherry expression. **(f)** Representative flow cytometry plots of mCherry-CART and BFP-fused 19BBz-tEGFR CART population frequencies following co-culture for 2 days. **(g and h)** Summary of f indicating percentage of mCherry+ cells (g) and MFI of mCherry signal (h). **(i and j)** Apoptosis of mCherry-CARTs from f was assessed using SYTOX and Annexin V staining. Data in e–j are representative of three independent experiments with samples from unique healthy donors. Error bars show mean ± SEM. Statistical comparisons were made using unpaired *t* tests. *P < 0.05 and **P < 0.01.

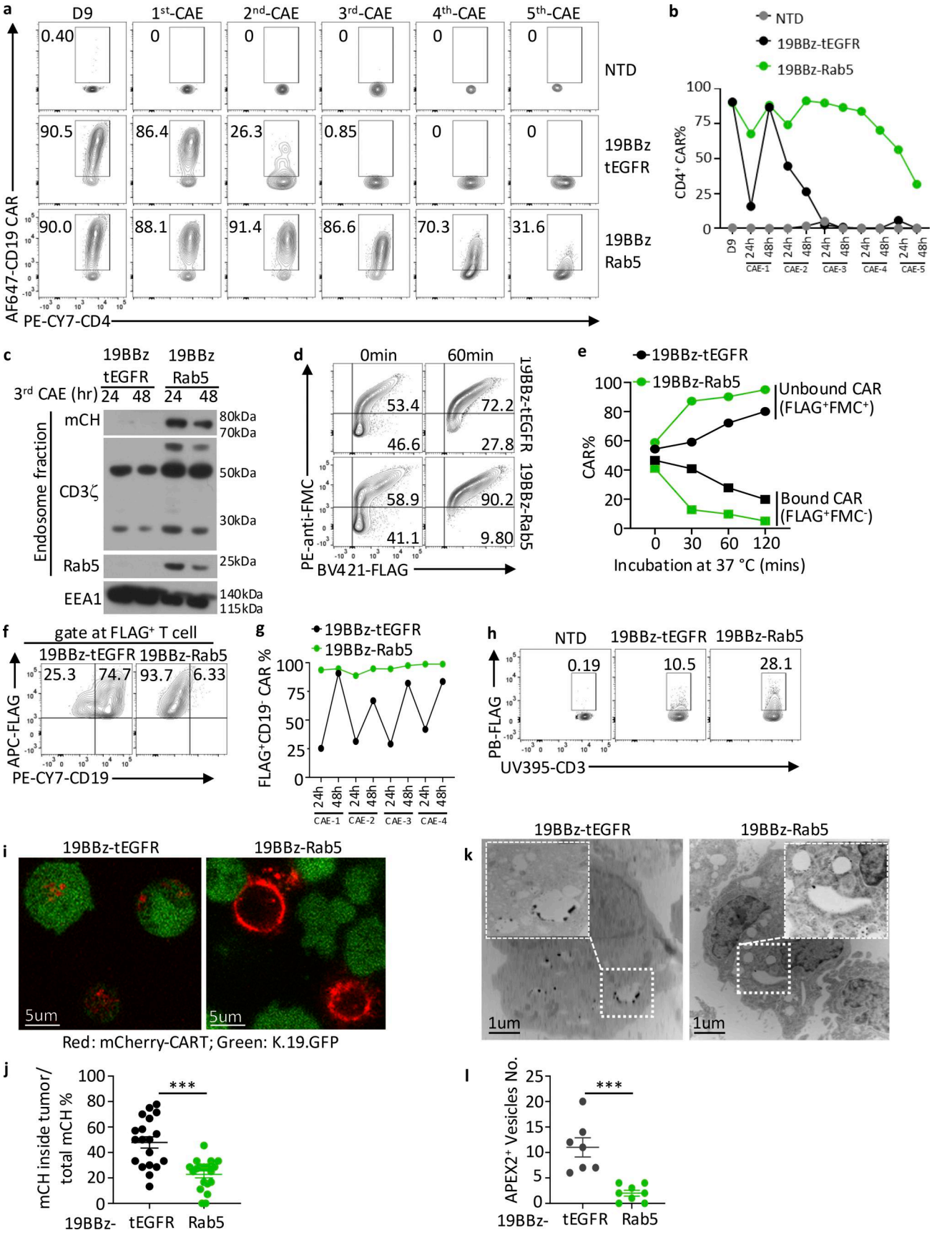

Figure 4. **Rab5 expression enables recycling of unbound CARs back to the CART surface. (a and b)** Representative flow cytometry plots of CAR expression in CD4+ CARTs during CAE assay, detected by labeled CD19 protein. Data are representative of three independent experiments with samples from

unique healthy donors. **(c)** Western blot showing CAR molecules in early endosome fraction purified from mCherry-fused 19BBz-tEGFR and 19BBz-Rab5 CARTs collected during the third-round CAE assay at the indicated time points. Data are representative of two independent experiments using samples from different healthy donors. **(d and e)** See Fig. S4 a for detailed workflow. Measurement of CD19-bound FLAG-CAR ($FLAG^+FMC63^-$) and CD19-unbound FLAG-CAR ($FLAG^+FMC63^+$) on CARTs, indicated by representative flow cytometry plots (d) and summary data (e). Data are representative of three independent experiments with samples from different healthy donors. **(f and g)** CD19-unbound CARs were measured with FLAG-tag–fused control or Rab5-CARTs during the CAE assay. CARTs were gated on APC-$FLAG^+$ populations before subsequent analysis of unbound CAR levels via anti-CD19 antibody staining using flow cytometry. Data are representative of two independent experiments with samples from unique healthy donors. **(h)** Surface CAR expression level measured staining of FLAG Ab after 48 h of the third-round CAE assay. Data are representative of three independent experiments. **(i and j)** Confocal imaging of the subcellular CAR (red) distribution 24 h after 19BBz-mCherry-tEGFR or -Rab5 CARTs co-cultured with K.19.GFP (green) (i), quantification of the percentage of mCherry-CAR internalization into tumor cells (j). Data are representative of three independent experiments with samples from unique healthy donors. **(k and l)** TEM images revealing the subcellular localization of engineered APEX2-tagged CAR molecules (black electron-dense deposits; k) within tumor cells. K.19.GFP cells were co-cultured with APEX2-fused control or Rab5 CARTs for 24 h, followed by T cell depletion and fixation. Samples were incubated with DAB and hydrogen peroxide to generate electron-dense APEX2 reaction products, and TEM images of K.19.GFP cells were captured. Quantification of the mean number of APEX2-CAR–positive vesicles per tumor cells is shown (l). Experiments are representative of five independent experiments. Error bars show mean ± SEM. Statistical comparisons were made using unpaired *t* tests. ***P < 0.001. Source data are available for this figure: SourceData F4.

microscopy (TEM). Likewise, tumors incubated with Rab5-CARTs internalized fewer APEX2-tagged CARs compared with controls (Fig. 4, k and l). These findings indicate that Rab5 helps maintain functional CAR on CARTs surface through two complementary mechanisms: firstly, Rab5 promotes CAR–CD19 complex internalization, which leads to dissociation of the CAR from CD19 and subsequent recycling of unbound CARs back to the cell surface; secondly, Rab5 expression prevents tumor-mediated trogocytosis of CARs from the CART surface. These two processes preserve a pool of unengaged, functional CARs (Fig. S4 c) for sustained tumor engagement.

Introduction of Rab5 into CARTs isolated from patients improves CART function

Next, we asked whether bidirectional transfer of antigen and CARs occurs within the human tumor microenvironment and if this process could be counteracted by Rab5 expression. We first confirmed that Rab5 exerted a similar effect on B cell maturation antigen (BCMA)-targeting CARTs (BCMABBz) co-cultured with H929 cells, in terms of enhancing tumor control, reducing trogocytosed antigen, and preserving functional CAR expression (Fig. 5, a–c). We then analyzed bone marrow aspirates from multiple myeloma (MM) patients collected 7–10 days after infusion of BCMABBz CARTs (Garfall et al., 2023). To test whether Rab5 could alter CARTs function in patient-derived cells, we generated mRNA constructs encoding either tEGFR (control) or Rab5 and electroporated them into resting bone marrow aspirates, which contained both CARTs and tumor cells. After 24 h, Rab5-electroporated CARTs displayed a significantly higher ability to bind BCMA protein compared with the tEGFR control (Fig. 5, d and e). This suggests that Rab5 overexpression can boost CARTs function in a tumor microenvironment. We next asked whether Rab5 could help CARTs resist relapse upon tumor rechallenge. Patient-derived CARTs were purified from bone marrow samples, electroporated with either control or Rab5 mRNA, and subsequently co-cultured with H929 or KMS-27 myeloma cell lines. Impressively, Rab5-expressing patient CARTs exhibited improved tumor-killing capacity (Fig.5 f), accompanied by reduced antigen trogocytosis and greater maintenance of surface CARs (Fig. 5, g and h). In summary, these results demonstrate that Rab5 expression restored CART function and improved antigen clearance in patient-derived CARTs.

Rab5 overexpression enhances the ability of CARTs to control solid tumors

By promoting antigen clearance from CARTs and preserving CAR surface expression, Rab5-expressing CARTs display enhanced functionality *in vitro*. To ascertain whether Rab5 expression improves *in vivo* activity, we established NALM6 tumors in NSG mice and infused either control and Rab5-expressing CD19-specific CARTs. Rab5-expressing CARTs more effectively controlled tumor growth than control CARTs, consistent with improved mouse survival (Fig. 6, a and b) and reduced residual tumor cells in the peripheral blood (PB) of Nalm6-bearing mice (Fig. 6, c and d). To further evaluate the antitumor activity of Rab5-expressing CARTs in a more challenging environment, we infused K.19.GFP cells into the flanks of NSG mice where they grow as solid tumors (Kim et al., 2022) (Fig. S5 a). Mice were then treated with non-transduced T cells (NTDs), 19BBz-tEGFR or 19BBz-Rab5 CARTs. Remarkably, Rab5-CARTs eradicated tumors both rapidly and completely (Fig. 6, e and f) and significantly improved survival compared with control mice (Fig. 6 g). In a separate experiment, tumors were isolated before they were cleared so we could study CARTs within the tumor microenvironment (Fig. 6, h and i). Rab5-CARTs retained significantly higher levels of surface CAR compared with control CARTs (Fig. 6, j and k), despite both groups having comparable CAR expression prior to infusion (Fig. S5 b). Clinical studies suggest that the presence of $CD4^+$ CARTs correlate with durable remission (Melenhorst et al., 2022). Interestingly, $CD4^+$ CARTs derived greater benefit from Rab5 expression than $CD8^+$ CARTs within the tumor microenvironment (Fig. S5, c–e). This correlated with superior CART persistence in mice treated with Rab5-CARTs compared with controls (Fig. 6, l and m), a phenotype also observed in PB (Fig. S5, f and g).

We next investigated whether Rab5 could enhance the efficacy of CART therapy against mesothelioma, a clinically relevant solid tumor. Mesothelin-targeting CARTs (MESOBBz-CARs) have shown promising activity in a phase I clinical trial (Walker et al., 2017) but durable cures remain elusive. We first developed and validated an *in vitro* model to test whether Rab5 enhances MESOBBz-CARs activity using EMMESO tumor, a human mesothelioma cell line isolated from a patient's tumor and stably transduced to express human mesothelin that is challenging to control both *in vitro* and *in vivo* (Moon et al., 2014). MESOBBz-

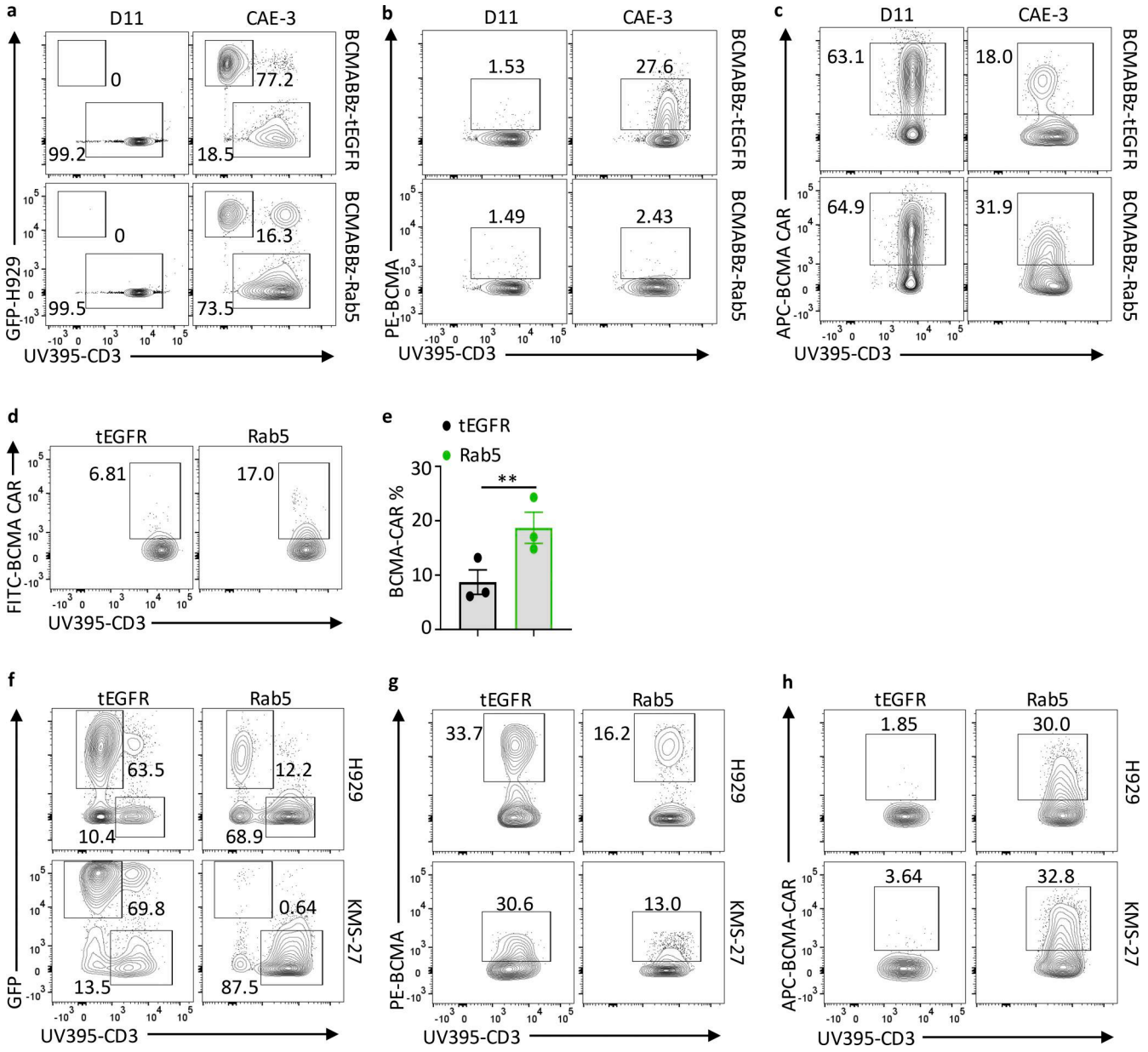

Figure 5. **Introduction of Rab5 into CARTs isolated from patients improves CART function. (a–c)** Primary human T cells were activated and transduced with BCMABBz-CAR expressing either tEGFR or Rab5. After 11 days of culture, 1 × 10^6 CAR$^+$ T cells were co-cultured with 2 × 10^6 H929-GFP cells. Flow cytometry measuring the persistence of GFP-expressing H929 cells and BCMA-specific CARTs before start of CAE assay and after the third tumor challenge (a), BCMA antigen on T cells (b), and surface CAR expression (c). Data are representative of three independent experiments with samples from different healthy donors. **(d and e)** Representative flow cytometry plots (d) and summary data (e) of BCMA CAR expression in T cells from BCMA-CART–treated MM patients, electroporated with Rab5 or tEGFR encoding mRNA. **(f–h)** T cells isolated from MM patients previously treated with BCMA-CART therapy were electroporated with tEGFR or Rab5 mRNA, then co-cultured with H929-GFP or KMS-27-GFP tumor cells for 48 h. Tumor elimination capability (f), BCMA expression level (g), and surface BCMA-CAR expression level (h) of patients-derived CARTs, measured by flow cytometry. Experiments in d–h are reproducible with three different donors. Error bar show mean ± SEM. Statistical comparisons were made using unpaired *t* tests. **P < 0.01.

Rab5 CARTs successfully cleared EMMESO co-cultures, whereas EMMESO cells were never completely cleared from the culture by control MESOBBz CARTs (Fig. 7, a and b), highlighting the importance of Rab5 expression in the treatment of solid tumors. Next, EMMESO tumor-bearing NSG mice were treated with NTD, MESOBBz-tEGFR, or Rab5 CARTs (Fig. S5 h). Compared with control CARTs, MESOBBz-Rab5 CARTs cleared tumors much more rapidly in all tumor-bearing mice (Fig. 7 c), without causing a significant reduction in body weight (Fig. S5 i). In a parallel experiment, we isolated tumors 21 days post-CART infusion. Tumors from Rab5-CART–treated mice were significantly smaller (Fig. 7 d) and contained more tumor-infiltrating CARTs (Fig. S5, j and k). Mechanistically, Rab5 expression reduced the uptake of tumor-derived material into CARTs (Fig. 7, e and f) and enhanced surface CAR expression (Fig. 7, g and h). Again, CD4$^+$ T cells more significantly benefited from Rab5 in terms of maintaining higher

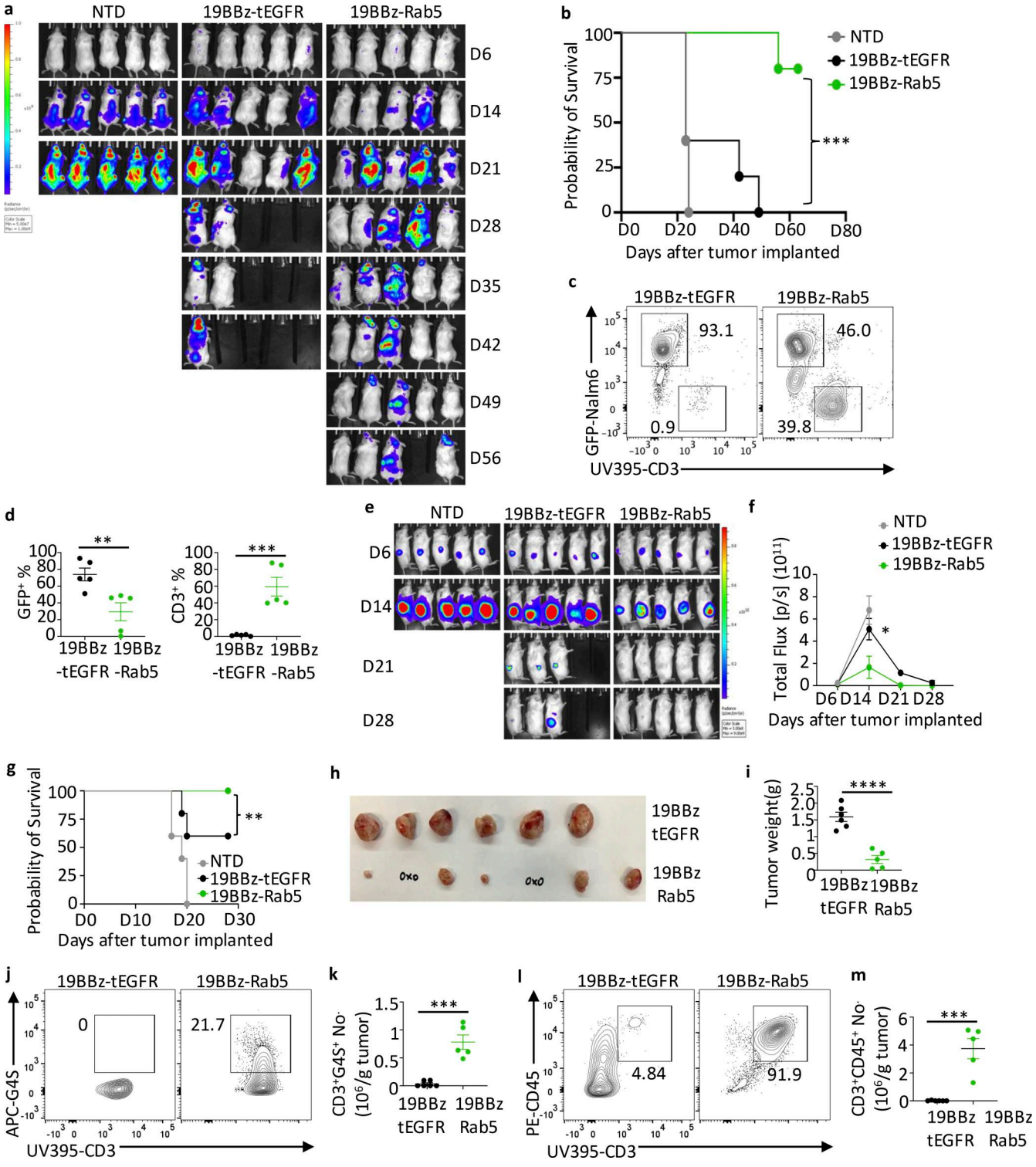

Figure 6. **Rab5 CARTs exhibit superior *in vivo* antitumor efficacy. (a)** NSG mice were intravenously injected with 1 × 10^6 Nalm6 tumor cells. 7 days later, mice received 1 × 10^6 NTDs or the indicated CD19-specific CARTs. Tumor progression was monitored weekly by bioluminescent imaging (BLI). **(b)** Survival of Nalm6-bearing mice following infusion of the indicated CARTs. Data in a and b are representative of two independent experiments, *n* = 5 mice for each group. **(c and d)** Residual tumor cells and T cells in PB from mice in a were analyzed by flow cytometry on day 22 after tumor injection. Data are representative of two independent experiments, *n* = 5. **(e)** 1 × 10^6 K.19.GFP cells were injected s.c. into NSG mice. 7 days later, 1 × 10^6 of the indicated T cells were infused. Tumor progression was monitored weekly using BLI for tumor-bearing NSG mice treated with the indicated 19BBz CARTs. **(f)** Tumor burden and statistical analyses of e. Total flux was quantified as the total photon count of each mouse. **(g)** Survival curve of tumor bearing mice infused with the indicated CARTs. Data in e–g are representative of three independent experiments, *n* = 5 mice for each group. **(h and i)** Image (h) and weight (i) of day 14 tumor tissues isolated from mice treated with 19BBz-tEGFR or 19BBz-Rab5 CARTs. Data are representative of two independent experiments, *n* = 6–7 mice for each group. **(j and k)** CAR surface expression of tumor-infiltrating CARTs 14 days after infusion. **(l and m)** CART expansion (l) and absolute number (m) of CAR-positive $CD3^+$ T cells isolated from

tumors after 14 days CARTs infusion. Data in j–m are representative of two independent experiments, n = 5-6 mice for each group. Error bars show mean ± SEM. Statistical comparisons were made using unpaired t tests. *P < 0.05, **P < 0.01, ***P < 0.001, and ****P < 0.0001. In b and g, survival curves were compared using the log-rank Mantel–Cox test.

CAR surface expression in the tumor microenvironment (Fig. S5, l and m). Rab5 did not affect CART checkpoint marker expression (Fig. S5 n), consistent with *in vitro* observations. As a final test of the function of Rab5-expressing CARTs in solid tumors, we employed an *in vivo* model using AsPC-1 cells, a tumor line that naturally expresses mesothelin. Following infusion of control or Rab5-expressing MESOBBz CARTs, similar results to the EM-MESO model were observed. Rab5-expressing CARTs exhibited superior control of tumor growth compared with control CART treatment (Fig. 7, i and j). This enhanced antitumor activity was consistent with increased CART expansion within the tumor microenvironment (Fig. 7, k and l), as well as higher levels of surface CAR, supporting sustained tumor cell killing (Fig. 7, m and n). Together, these data confirm that Rab5 engineering markedly enhances CART therapeutic efficacy against solid tumors *in vivo*.

Discussion

Trogocytosis serves as a key mechanism of immune modulation within the tumor microenvironment (Kim et al., 2025). Unlike phagocytosis, trogocytosis maintains the functionality of the exchanged molecules, potentially influencing the balance of molecules that potentiate (CD86 or 4-1BBL) or inhibit (TIM-3, HLA-G and PD-L1) immune cell activation (Hwang et al., 2000; Pagliano et al., 2022; Shin et al., 2021; Tekguc et al., 2021). Engineering T cells to express CARs introduces additional complexities related to trogocytosis (Hamieh et al., 2019). CARTs can trogocytose their target antigen, resulting in fratricide. It is important to note that although natural CD8 T cells can acquire cognate pMHC from APCs or tumor cells, making them susceptible to fratricide (Huang et al., 1999); the threat CARTs face from fratricide differs substantially from that of natural T cells acquiring pMHC. While tumors typically present only hundreds of cognate pMHC molecules on their cell surface (Kim et al., 2022; Stopfer et al., 2020), the number of target antigens that can be captured by CARTs can be orders of magnitude higher, increasing the risk of fratricide (Cappell and Kochenderfer, 2021; Malik-Chaudhry et al., 2021). Likewise, because trogocytosis is bidirectional, large numbers of CARs can also be transferred to tumors, leading to a reduction of surface CAR levels on the T cell that facilitates immune escape (Zhai et al., 2023), especially since CARTs are less sensitive to target antigen than natural T cells (Anikeeva et al., 2021; Burton et al., 2023). In endogenous T cells, TCR loss is minimal due to limited cognate pMHC abundance on target cells (Huang et al., 2013; Stinchcombe et al., 2023), but in CARTs, this loss is substantial and results in significant dysfunction. In addition to trogocytosis, high-affinity CAR interactions with their target can block subsequent CAR binding to new tumor cells. Together, fratricide, CAR loss, and CAR blocking represent mechanisms of CARTs dysfunction. Lower affinity CAR binders have been shown to be less susceptible to fratricide since target antigen may not be so readily captured by the CART (Olson et al., 2022). We would speculate that if the binders confer similar activity to the CARTs, then combining the lower affinity binder with ectopic Rab5 expression would synergize to further reduce CART dysfunction and fratricide.

Our study reveals that maintenance of endocytic activity can counteract the dysfunction caused by trogocytosis. Endocytosis removes trogocytosed antigen from the CART surface, preventing fratricide; limits CAR capture by tumors, maintaining more surface CARs; and facilitates the internalization of antigen-bound CARs, allowing antigen dissociation and recycling of unbound CARs to the cell surface. Curiously, CARTs lose endocytic activity after CAE, exacerbating the effects of CART dysfunction.

Endocytosis involves at least five distinct pathways and over 60 proteins that collaboratively regulate the lipid and protein composition of the cell membrane (Zerial and McBride, 2001). We found that Rab5 expression is necessary to maintain endocytic activity. The importance of Rab5 in CART biology is underscored by our finding that expression of a GTPase-mutated, dominant-negative version of Rab5 rapidly abolished CART activity. Conversely, expression of Rab5 was sufficient to enhance endocytic activity, suggesting that Rab5 functions as a rate-limiting component of endocytic activity in CARTs. Importantly, Rab5 overexpression did not induce global changes in gene expression, indicating that its effect is primarily on maintaining endocytic activity within the CART without affecting other transcriptional processes. Traditionally, endocytosis is considered a mechanism of receptor downregulation. Our findings reveal a complementary role in the context of sustained tumor interactions where endocytosis preserves unbound CAR surface persistence. Parallels may exist with the Notch pathway, in which endocytosed ligands recycle back to the cell surface to enable continued signaling (Le Borgne and Schweisguth, 2003).

Rab5-CARTs showed striking therapeutic activity in several preclinical models. Introduction of Rab5 via RNA transfection into patient-derived bone marrow cells markedly improved the function of these minimally manipulated CARTs, suggesting that transient delivery of Rab5 via mRNA-LNPs may be an effective way to reinvigorate CART activity. Tumor-bearing humanized mice treated with Rab5-CARTs cleared tumors quickly and prevented relapse over time. Examination of CARTs within these tumors confirmed all the findings of our *in vitro* studies: we observed less trogocytosed antigen on Rab5-CARTs and much higher levels of available CAR to bind new targets. These data provide the basis and rationale to use Rab5-CARTs in the clinic.

In summary, we identified a therapeutic strategy to counteract trogocytosis-driven target antigen accumulation and CAR downregulation. Engineering CARTs with Rab5 prevents fratricide, preserves unbound CAR on the cell surface, and markedly

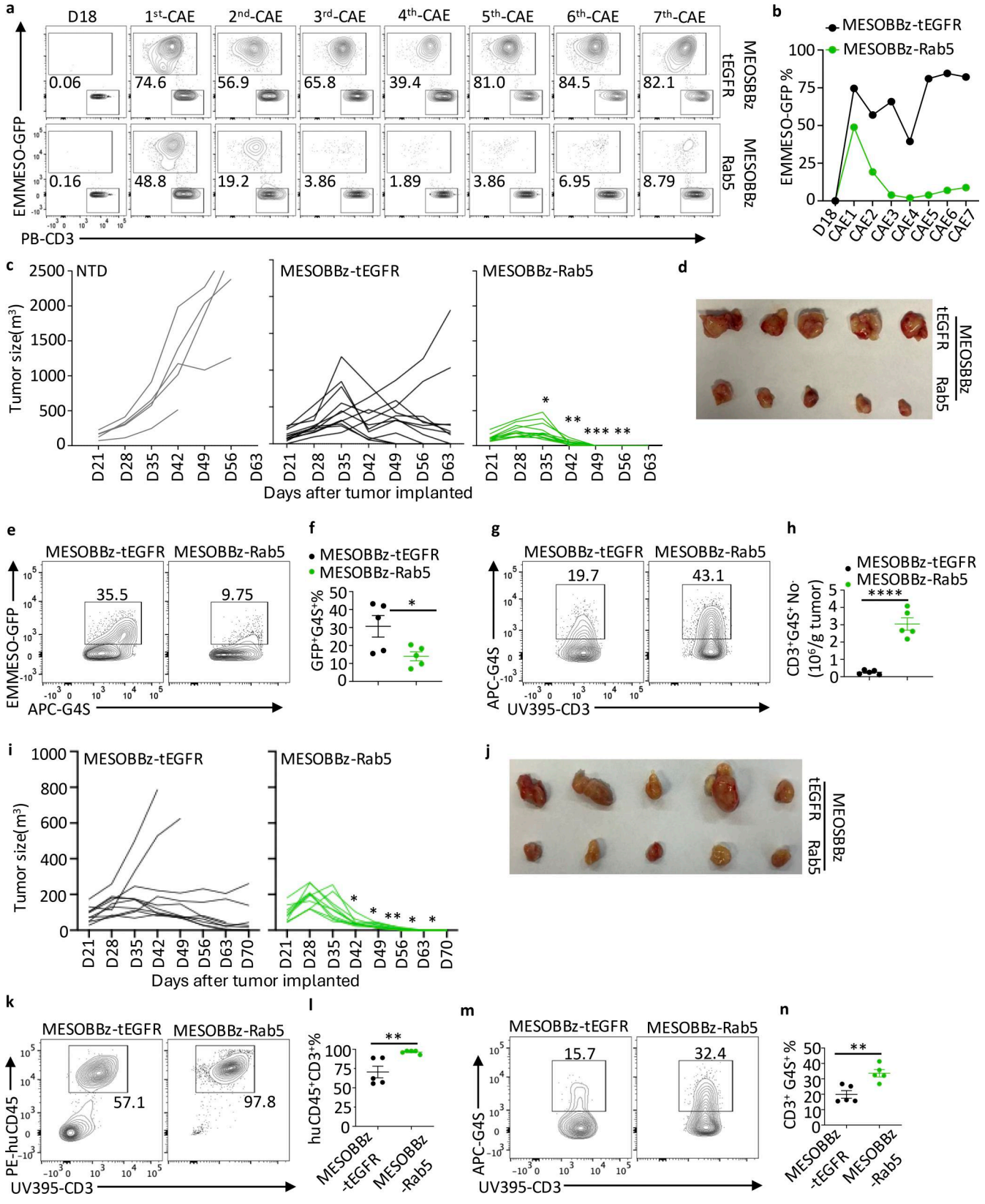

Figure 7. **Rab5 expression enhances the ability of CARTs to control solid tumors. (a and b)** Primary human T cells were activated and transduced with MesoBBz-CAR expressing either tEGFR or Rab5. After 18 days of culture, 1 × 10^6 CAR⁺ T cells were co-cultured with 2 × 10^6 GFP⁺ EMMESO cells. Representative flow cytometry plots (a) and summary (b) of GFP⁺ EMMESO populations throughout the CAE assay. Data are representative of three independent experiments with samples from different healthy donors. **(c)** Individual EMMESO tumor sizes in mice infused with the indicated MESOBBz CARTs, measured weekly. Data are representative of three independent experiments, *n* = 5–11 mice for each group. **(d)** Representative images of EMMESO tumor tissues isolated 21 days after

infusion from mice treated with MESOBBz-tEGFR or MESOBBz-Rab5 CARTs. Data are representative of two independent experiments, n = 5 mice for each group. **(e and f)** Tumor-bound MESOBBz CARs, detected in tumor-infiltrating control or Rab5 CARTs 21 days after infusion, using tumor samples from d. Data are representative of two independent experiments, n = 5 mice for each group. **(g and h)** Surface CAR expression 21 days after MESOBBz-tEGFR or MESOBBz-Rab5 CARTs infusion, assessed by anti-G4S linker antibody staining in tumor samples from d. Data are representative of two independent experiments, n = 5 mice for each group. **(i)** Individual AsPC-1 tumor sizes in mice infused with the MESOBBz CARTs, measured weekly. NSG mice were injected s.c, with 1×10^6 AsPC-1 cells. After 21 days, tumor-bearing mice were infused with 0.5×10^6 MESOBBz-tEGFR or MESOBBz-Rab5 CAR T cells. Data are representative of two independent experiments, n = 10 mice per group. **(j)** Representative images of AsPC-1 tumor tissues isolated 21 days after MESOBBz-tEGFR or MESOBBz-Rab5 CARTs infusion. Data are representative of two independent experiments, n = 5 mice for each group. **(k and l)** Expansion of tumor-infiltrating CARTs was assessed 21 days after infusion using tumor samples from j. **(m and n)** Surface CAR expression on tumor-infiltrating CARTs was measured 21 days after infusion using tumor samples from j. Data are representative of two independent experiments, n = 5 mice for each group. Error bars show mean ± SEM. Statistical comparisons were made using unpaired t tests. *P < 0.05, **P < 0.01, ***P < 0.001, and ****P < 0.0001.

enhances antitumor efficacy. This approach of augmenting membrane trafficking not only sustains CART persistence and function under chronic tumor exposure but may also offer a broadly applicable strategy to improve the durability and effectiveness of adoptive T cell therapies.

Materials and methods

Cell lines

The human myelogenous leukemia cell line K562 was transduced with a lentiviral vector encoding pTRPE-huCD19-CBG-GFP minigenes (K.19.GFP). Single-cell clones were sorted, and a clone that exhibited stable expression was selected as previously described (Milone et al., 2009). Human EM-Meso-GFP-Luc cell line (EMMESO-GFP) (Moon et al., 2014) was a kind gift from Dr. Steven M. Albelda laboratory (University of Pennsylvania, Philadelphia, PA, USA). AsPC-1, H929, and KMS-27 cell lines are gift from Dr. Carl June laboratory (University of Pennsylvania, Philadelphia, PA, USA). K.19.GFP, EMMESO-GFP, AsPC-1, H929, and KMS-27 cells were cultured in R10 media consisting of RPMI-1640 (Gibco) with 10% fetal bovine serum (Avantor Seradigm), 1% HEPES (Gibco), 1% GlutaMAX (Gibco), and 1% penicillin/streptomycin (Gibco). All cell lines were free of mycoplasma contamination.

Mice studies

Animal experiments were performed according to protocols approved by the Institutional Animal Care and Use Committee (IACUC) of the University of Pennsylvania. 6- to 12-week-old female and male nonobese diabetic/severe combined immunodeficient/γ-chain$^{-/-}$ (NSG) mice were obtained from the Stem Cell and Xenograft Core (RRID: SCR_010035) of the Abramson Cancer Center at the University of Pennsylvania. Mice were maintained in pathogen-free conditions. Mice health status was routinely checked by qualified veterinarians.

Human samples

De-identified healthy donor primary T lymphocytes were provided by the Human Immunology Core (RRID: SCR_022380) at the University of Pennsylvania. De-identified post-CART-BCMA infusion bone marrow samples were collected from high-risk MM patients enrolled on a CART-BCMA clinical trial who consented that their cells could be used for research (Garfall et al., 2023).

Viral vector construction

pTRPE 19BBζ T2A GFP and pTRPE 1928z T2A GFP are third generation lentiviral vectors that expresses a CD19-specific CAR that uses the 4-1BB or CD28 and CD3z (ζ) signaling domains linked via T2A to GFP (Leibman et al., 2017; Shukla et al., 2025b). pTRPE 19BBz T2A Rab5 or pTRPE 19BBz T2A tEGFR was generated by replacing GFP with a gblock (IDT) containing the coding sequence of Rab5 (GenBank U18420.1), the S35N Rab5 dominant-negative mutant, Rab4 (GenBank M28211.1), Rab11 (GenBank AF000231.1), or tEGFR. The anti-MESO (M5) CAR (Good et al., 2021) was a gift from Dr. Carl H. June (University of Pennsylvania, Philadelphia, PA, USA) and their Rab5 or tEGFR co-expressing constructs were generated in similar manner as described above. mCherry, BFP, or APEX2 was fused to the C terminus of the CD3ζ chain. A FLAG tag was inserted right before the transmembrane region, enabling direct detection of surface CAR molecules. To construct a BCMA-specific CAR, a llama was immunized with the extracellular domain of BCMA, a variable heavy domain of heavy chain (VHH) phage display library comprising ~14 billion members was constructed and serially screened for BCMA binding as previously described (Bhoj et al., 2021). From this, 100 million VHH BCMA binders were isolated. 54 of these were randomly picked and 34 of 54 had unique sequences. CARs linking these binders to the 4-1BB and CD3 zeta chain were generated, and CARs containing clone 20A conferred the most potent activity against BCMA tumor lines. All final constructs were verified using restriction digests and whole plasmid sequencing (Plasmidsaurus).

Lentiviral vector production

HEK293T cells were transfected with lentiviral CAR transfer plasmid and packaging plasmids using Lipofectamine 2000 (Invitrogen) following the manufacturer's protocol. Lentiviral supernatants were collected 24 and 48 h after transfection and concentrated using high-speed ultracentrifugation as previously described (Shukla et al., 2025a). The resulting concentrated lentivirus batches were resuspended in cold R10 media and stored at −80°C.

CART generation

CARTs were generated as previously described (Medvec et al., 2018). Briefly, CD4$^+$ and CD8$^+$ human T cells mixed at 1:1 ratio and plated at 1×10^6 total T cells/ml were activated with huCD3/CD28 Dynabeads (Gibco) at a 3:1 bead-to-cell ratio. The following day, T cells were transduced with lentiviral vectors by adding

the virus supernatant directly to T cell cultures. These cultures were maintained in Cell Therapy Systems (CTS), OpTmizer T Cell Expansion Serum Free Medium (Thermo Fisher Scientific) supplemented with CTS OpTmizer T cells Expansion Supplement (Thermo Fisher Scientific), 1% GlutaMAX (Gibco), 1% penicillin/streptomycin (Gibco), and 1% HEPES (Gibco). After 3 days, beads were removed from the cell culture. For the remainder of the culture, cells were counted every other day and maintained at 0.5 × 10^6 cells/ml.

CAE assay

A total of 2 × 10^6 K.19.GFP cells, GFP-expressing-KMS-27, NCI-H929 (Sun et al., 2024), or EMMESO (Moon et al., 2014) cells were co-cultured with 1 × 10^6 CAR-positive T cells in 1 ml OpTmizer T Cell Expansion Medium in a 12-well plate. Every 24 h, cells were harvested for flow cytometry analysis of surface CAR expression and the presence of tumor. Fresh culture medium (0.5 ml) was then added to the remaining cells. Every 48 h, surface CAR expression and tumor cell survival were monitored as above. Subsequently, an additional 2 × 10^6 tumor cells resuspended in 0.5 ml fresh medium were added to the ongoing co-culture.

RNA synthesis, electroporation of patient-derived CARTs, and detection of BCMA-CAR

Construction of mRNA vector, RNA *in vitro* transcription (IVT), and RNA electroporation were performed as previously described (Wei et al., 2013). Briefly, the tEGFR and Rab5 coding sequence were cloned into an IVT vector containing T7 promoter, 5′ and-3′ UTR elements, and poly(A) tail. mRNA was synthesized and purified with mMESSAGE mMACHINE T7 ULTRA Kit and MEGAclear Kit (Invitrogen) followed the instructions, verified by agarose gel electrophoresis, aliquoted, and stored at −80°C. CARTs were isolated from MM patient bone marrow (Garfall et al., 2023) using the Dynabeads Untouched Human T Cells Kit (Invitrogen). Purified T cells were washed and resuspended in OPTI-MEM (Invitrogen) and electroporated with 5 µg of IVT RNA. 6 h after electroporation, CARTs were co-cultured with indicated tumor cells. Tumor control, BCMA, and BCMA-CAR on the cell surface were analyzed at by flow cytometry.

Measurement of unbound CAR

FLAG-tagged CD19-BBz CARTs were incubated with AF647-conjugated CD19 protein at 37°C for 1 h to allow the formation of CD19–CAR complexes, followed by endocytosis and potential dissociation. Cells were then washed with ice-cold PBS. To track the recycling of CD19-released CARs, cells were incubated with anti-FMC63 antibody, which recognizes the scFv domain of CD19BBz-CARs, at 37°C for 0, 30, 60, or 120 min. Internalized CARs that were released from CD19 and recycled back to the cell surface in an unengaged state were identified as double positive for both anti-FLAG and anti-FMC63 staining by flow cytometry.

Measurement of endocytic activity

For endocytosis measurement using AM1-44 dye, 5 µM freshly prepared AM1-44 was added to rested CARTs or those collected from the CAE assay and incubated at 37°C for 1 h. Cells were then washed with PBS and fixed with 2% pre-warmed paraformaldehyde (PFA) at room temperature (RT) for 15 min. After fixation, cells were stained with the indicated dye or antibodies to identify the cell membrane or nucleus. The samples were then imaged using confocal microscopy. To measure endocytic activity by tracking pHrodo Dextran uptake, CARTs treated with or without tumor cells were incubated with 20 µg/ml pHrodo Red Dextran at 37°C for 20 min in serum-free culture buffer, followed by washing with pre-warmed PBS. The samples were then analyzed by flow cytometry.

Fratricide assay

mCherry-fused control or Rab5 CARTs were co-cultured with K.19.GFP cells for 24 h to facilitate CD19 transfer to the CARTs. These CD19-bearing CARTs were then co-cultured with BFP-fused 19BBz-tEGFR CARTs for 2 days. Following co-culture, the reduction in the mCherry-positive population was assessed to evaluate fratricide mediated by BFP-CARTs. Additionally, CD19 expression levels on both mCherry-fused donor CARTs and BFP-fused recipient CARTs were measured using flow cytometry.

Flow cytometry

CD19 CAR expression was assessed using AF647-labeled CD19 protein (0.5 µg/ml) or AF647-G4S linker antibody (1:400). MESO CAR expression was assessed using AF647-labeled MSLN protein (1 µg/ml) for *in vitro* assays or AF647-G4S linker antibody (1:400) for *in vivo* detection. For staining of other surface markers, cells were incubated with a 1:200 dilution of antibodies at 4°C for 30 min in FACS buffer (PBS + 0.5% FBS). For intracellular staining, cells were first fixed and permeabilized with BD Cytofix/Cytoperm solution (BD Biosciences) at 4°C for 20 min, followed by staining at 4°C for 30 min in the dark. Flow cytometry data were acquired using BD LSRFortessa (BD Biosciences) and analyzed with FlowJo software (BD Biosciences).

Western blotting and early endosome fraction isolation

T cells were lysed with 1× Lysis Buffer (CST) containing Protease Inhibitor Cocktail (Thermo Fisher Scientific) for 10 min on ice. Lysed cells were then centrifuged at 12,000 rpm for 10 min at 4°C, and the supernatant was collected for immunoblot assays. For analysis of CARs in endosomes, early endosomes from T cells were isolated using the Trident Endosome Isolation Kit (GeneTex) according to the manufacturer's instructions. Briefly, T cells were first purified from the tumor rechallenge co-cultures using the Dynabeads Untouched Human T Cells Kit (Invitrogen). After washing with cold PBS, the cell pellet was prepared for endosome isolation following the manufacturer's protocol. All procedures were performed on ice or at 4°C. The early endosome pellets were resuspended in 80 µl of 1× lysis buffer (CST) for immunoblotting analysis.

Confocal imaging

mCherry-fused CARTs were incubated with GFP-fused K562 cells at 1:1 ratio of total 1 × 10^6 cells for the indicated amount of time. For high-content imaging of mCherry-CAR molecules, CARTs were stained with CellMask Deep Red Actin Tracking

Stain (Invitrogen) and Hoechst 33342 (Thermo Fisher Scientific) or anti-CD45 antibody (Bio-Techne) for 15 min at RT, followed by three washes with PBS. All the cells were fixed with 2% methanol-free PFA buffer for 30 min at RT and then washed three times with pre-warmed PBS. The cells were then transferred to glass-bottom dishes (ibidi) and mounted with ProLong Glass Antifade Mountant (Invitrogen). Imaging was performed using a Leica Stellaris 8 Falcon FLIM confocal microscope with a 40× (1.30 NA) or a 100× (1.40 NA) oil immersion objective lens. Captured images were analyzed using LASX software.

TEM

For TEM, 1 × 10^6 APEX2-fused CARTs were co-cultured with 2 × 10^6 K.19.GFP cells for the indicated period. CART and tumor populations were analyzed individually. To facilitate this, CARTs were separated using the Dynabeads CD3 kit (Invitrogen) according to the manufacturer's instructions. The CD3 negative (tumor cells) population was retained for analysis. Purified cells were fixed with 2% PFA solution and 2.5% glutaraldehyde solution at 4°C for at least 2 h. Samples were then prepared for diaminobenzidine (DAB) staining as previously described (Stinchcombe et al., 2023). Briefly, fixed cells were washed with pre-cold 0.1M sodium cacodylate rinsed in 0.5 M Tris-HCl buffer (pH 7.6) and incubated in DAB reaction solution (0.75 mg/ml DAB dissolved in HCl and 0.3% vol/vol hydrogen peroxide in Tris-HCl buffer) for 20 min at 4°C in the dark. Samples were washed in Tris-HCl buffer, followed by 0.1 M sodium cacodylate, and then post-fixed in 0.1% osmium tetroxide for 1 h at 4°C. After washing with pre-cold distilled H_2O (dH_2O), samples were stained with 0.5% aqueous uranyl acetate overnight at 4°C. The next day, samples were dehydrated with graded concentrations of ethanol (50, 70, 80, 90, and 100%) and embedded in 1:1 and subsequently pure EPON resin overnight at RT. Ultrathin sections were prepared by the Electron Microscopy Resource Lab (RRID: SCR_022375) at the University of Pennsylvania. Sections were imaged with a JEOL JEM 1010 transmission electron microscope.

Bulk RNA-seq and data analysis

Human T cells from four different healthy donors were activated with anti-CD3/28–coated beads and transduced with either 19BBz-tEGFR or 19BBz-Rab5 vectors. CARTs expanded *in vitro* for 9 days or CARTs co-cultured with K.19.GFP cells at a 1:2 ratio (CARTs:Targets) were isolated for analysis. With CAE-CARTs, 48 h after the third round of target rechallenge, $CD3^+CAR^+$ cells were enriched. Dead cells were removed using the Dead Cell Removal Kit (Miltenyi Biotec). T cells were isolated from target K562 cells using the Dynabeads Untouched Human T Cells Kit (Invitrogen). Surface CAR-positive cells were sorted by flow cytometry. A portion of each sample was reserved to test Rab5 overexpression via immunoblotting. For RNA-seq analysis, another portion (1 × 10^6 cells per sample) was flash-frozen in liquid nitrogen and sent to BGI Genomics for sample quality control, mRNA isolation, RNA library preparation, and sequencing. To address potential variability in genes with low read count, filtering was performed to omit genes in which more than four samples had a read count <10. Genes with an adjusted P value <0.05 were considered significant, and those with fold changes of >2 were defined as differentially expressed genes for the present study. Differential gene expression analysis was performed using DEseq2.

Xenograft mouse model

NSG mice were purchased from and housed in the Stem Cell and Xenograft Core of the Abramson Cancer Center (University of Pennsylvania), under pathogen-free conditions. Animal studies were approved by the University of Pennsylvania IACUC (protocol 807158). For the CD19-CART mouse model, NSG mice were s.c. injected with 1 × 10^6 K.19.GFP cells suspended in 100 µl Matrigel (CORNING): PBS (1:1) into the right flank. Six days after tumor implantation, 1 × 10^6 CAR-positive CD19-CARTs from 10 days of *in vitro* culture were i.v. injected into tumor-bearing mice. Tumor progression was monitored by bioluminescence imaging every 7 days. Body weight and survival conditions were checked weekly. For the MESO-CART mouse model, NSG mice were s.c. challenged with 1 × 10^6 EMMESO or AsPC-1 cells in the right flank. When the mean tumor volume reached 150 mm^3, mice were i.v. treated with 0.5 × 10^6 MESO-CAR-positive CARTs. Tumor volumes were calculated using caliper measurements. Tumor growth and body weight were assessed weekly. At the indicated days after CARTs infusion, mice were sacrificed, and tumors were harvested and digested with Tumor Dissociation Kit (Miltenyi Biotec) following the manufacturer's protocol. Tumor-infiltrating lymphocytes were processed with Lymphocyte Cell Separation Medium (Cedarlane) by centrifugation (1200 *g*, 20 mins). Spleen samples from tumor-bearing mice were prepared by mashing them through 100-µm filters (Falcon), followed by red blood cell lysis with ACK Lysis Buffer (Lonza). Peripheral blood samples were also treated with ACK Lysis Buffer for 10 min on ice. T cells from the above suspensions were identified by flow cytometry with anti-mouse $CD45^-$, anti-human $CD45^+$, and anti-human $CD3^+$ antibodies.

Study approval

All subjects provided written informed consent for their samples to be used as part of research studies. The study was reviewed and approved by the University of Pennsylvania Institutional Review Board (IRB). The regulatory sponsor was the University of Pennsylvania. The Human Immunology Core at the University of Pennsylvania maintains an IRB-approved protocol (705906) in which healthy individuals provide written consent for their apheresis material be used in research studies.

Statistical analysis

Significance of *in vivo* tumor-bearing mice survival data was calculated using the log-rank Mantel–Cox test. Statistical analyses on flow cytometry, confocal imaging, and TEM quantification were determined by unpaired *t* test. All values and error bars are presented as mean ± SEM. All statistical tests were performed using GraphPad 10.

Online supplemental material

Fig. S1 supports Fig. 1 by providing additional information on gene expression analysis and endocytosis. Fig. S2 describes the

vectors and T cells used to study Rab5 overexpression. Fig. S3 shows additional experiments using Rab5 mutants in CAE assay. Fig. S4 show confocal images indicating that Rab5 expression inhibits CAR trogocytosis into tumor cells, and Fig. S5 presents additional data comparing Rab5-CARTs and tEGFR-CARTs from *in vivo* experiments.

Data availability

Bulk-RNA seq data has been deposited at GEO: GSE269885 is publicly available as of the date of publication. Any additional information required to reanalyze the data reported in this paper is available from the lead contact upon request.

Acknowledgments

We thank the Human Immunology Core (RRID: SCR_022380) for providing purified human T cells; Biao Zuo and Inna Martynyuk of Electron Microscopy Resource Lab (RRID: SCR_022375) for providing advice and assistance of TEM preparation and imaging; Ruthel Gordon of Penn Vet Imaging Core (RRID: SCR_022764), which is supported by National Institutes of Health S10 OD032305-01A1, for high-resolution imaging; Stem Cell and Xenograft Core (RRID: SCR_010035) for providing and housing NSG mice; and Flow Cytometry and Cell Sorting Facility (RRID: SCR_022376) for cell sorting and maintaining flow cytometry daily. We also thank Drs. Carl H. June for MESO-BBz vector and for the suggestion to use samples from BCMA clinical trial; Steve Albelda for the EMMESO cell line; Edward A. Stadtmauer, Dan T. Vogl, Adam J. Waxman, Regina Ferthio, Anne Marie Nelson, and Kim-Marie Shea for their support of CAR-BCMA clinical trial; and David Barrett (Kite Pharma, Santa Monica, CA, USA), Gavin Ellis, Sriram Srivatsa, Yuqi Zhou, and John Wherry, (University of Pennsylvania, Philadelphia, PA, USA) for reagents and helpful advice.

Research supported by National Institutes of Health U19AI149680, UM1AI164570, and sponsor research from Tmunity/Kite Pharma.

Author contributions: Meidi Gu: conceptualization, data curation, formal analysis, investigation, methodology, project administration, validation, visualization, and writing—original draft, review, and editing. Kaitlin A. Read: data curation, formal analysis, visualization, and writing—review and editing. Vipin Bhardwaj: data curation, formal analysis, investigation, methodology, software, and visualization. Edmund J. Carvalho: data curation, investigation, and methodology. David Nardo: conceptualization, investigation, and methodology. Justin C. Shayne: formal analysis, investigation, visualization, and writing—review and editing. Divanshu Shukla: investigation. Wei Liu: resources and writing—review and editing. Donald L. Siegel: investigation, resources, and writing—review and editing. Neil C. Sheppard: resources and writing—review and editing. Michael C. Milone: methodology and writing—review and editing. Adam D. Cohen: resources and writing—review and editing. Alfred L. Garfall: resources and writing—review and editing. James L. Riley: conceptualization, funding acquisition, project administration, supervision, and writing—original draft, review, and editing.

Disclosures: M. Gu reported a patent to Augmenting CAR T cell activity pending "WO2025171295A1." N.C. Sheppard reported grants from ScaleReady; personal fees from BlueWhale Bio, Waypoint Bio,Pan Cancer T, UroGen Pharma, and Able Sciences; and "other" from CARTx Therapeutics; in addition, N.C. Sheppard had a patent to WO2024206569A2 pending. M.C. Milone reported "other" from Verismo Therapeutics and Cabaletta Bio outside the submitted work. A.L. Garfall reported grants from Novartis and NIH/NCI during the conduct of the study; and personal fees from Novartis, Johnson & Johnson, Regeneron, Gracell, AstraZeneca, Pfizer, BMS, MJH Life Sciences, DAVA Oncology, and Curio Science outside the submitted work; in addition, A.L. Garfall had a patent to US11747346B2 licensed "Novartis," a patent to US20200371091A1 pending, a patent to US20200360431A1 pending, and a patent to WO2024148212A2 pending. J.L. Riley reported grants, personal fees, and "other" from Tmunity/Kite Pharma/Gilead during the conduct of the study; and grants from BlueWhale Bio and "other" from BlueWhale Bio outside the submitted work; in addition, J.L. Riley had a patent to Augmenting car t cell activity pending and a patent to Augmenting car T cell activity licensed "Kite Pharma." No other disclosures were reported.

Submitted: 9 December 2025
Revised: 4 February 2026
Accepted: 26 March 2026

References

Andre, P., J. Boretto, A.O. Hueber, A. Regnier-Vigouroux, J.P. Gorvel, P. Ferrier, and P. Chavrier. 1997. A dominant-negative mutant of the Rab5 GTPase enhances T cell signaling by interfering with TCR down-modulation in transgenic mice. *J. Immunol.* 159:5253–5263.

Anikeeva, N., S. Panteleev, N.W. Mazzanti, M. Terai, T. Sato, and Y. Sykulev. 2021. Efficient killing of tumor cells by CAR-T cells requires greater number of engaged CARs than TCRs. *J. Biol. Chem.* 297:101033. https://doi.org/10.1016/j.jbc.2021.101033

Behnia, R., and S. Munro. 2005. Organelle identity and the signposts for membrane traffic. *Nature*. 438:597–604. https://doi.org/10.1038/nature04397

Bhoj, V.G., L. Li, K. Parvathaneni, Z. Zhang, S. Kacir, D. Arhontoulis, K. Zhou, B. McGettigan-Croce, S. Nunez-Cruz, G. Gulendran, et al. 2021. Adoptive T cell immunotherapy for medullary thyroid carcinoma targeting GDNF family receptor alpha 4. *Mol. Ther. Oncolytics*. 20:387–398. https://doi.org/10.1016/j.omto.2021.01.012

Birgisdottir, A.B., and T. Johansen. 2020. Autophagy and endocytosis - interconnections and interdependencies. *J. Cell Sci.* 133:jcs228114. https://doi.org/10.1242/jcs.228114

Bucci, C., R.G. Parton, I.H. Mather, H. Stunnenberg, K. Simons, B. Hoflack, and M. Zerial. 1992. The small GTPase rab5 functions as a regulatory factor in the early endocytic pathway. *Cell*. 70:715–728. https://doi.org/10.1016/0092-8674(92)90306-w

Burton, J., J.A. Siller-Farfan, J. Pettmann, B. Salzer, M. Kutuzov, P.A. van der Merwe, and O. Dushek. 2023. Inefficient exploitation of accessory receptors reduces the sensitivity of chimeric antigen receptors. *Proc. Natl. Acad. Sci. USA*. 120:e2216352120. https://doi.org/10.1073/pnas.2216352120

Cappell, K.M., and J.N. Kochenderfer. 2021. A comparison of chimeric antigen receptors containing CD28 versus 4-1BB costimulatory domains. *Nat. Rev. Clin. Oncol.* 18:715–727. https://doi.org/10.1038/s41571-021-00530-z

Cappell, K.M., and J.N. Kochenderfer. 2023. Long-term outcomes following CAR T cell therapy: What we know so far. *Nat. Rev. Clin. Oncol.* 20:359–371. https://doi.org/10.1038/s41571-023-00754-1

Chan, J.D., C.M. Scheffler, I. Munoz, K. Sek, J.N. Lee, Y.K. Huang, K.M. Yap, N.Y.L. Saw, J. Li, A.X.Y. Chen, et al. 2024. FOXO1 enhances CAR T cell stemness, metabolic fitness and efficacy. *Nature*. 629:201–210. https://doi.org/10.1038/s41586-024-07242-1

Charpentier, J.C., D. Chen, P.E. Lapinski, J. Turner, I. Grigorova, J.A. Swanson, and P.D. King. 2020. Macropinocytosis drives T cell growth by sustaining the activation of mTORC1. *Nat. Commun.* 11:180. https://doi.org/10.1038/s41467-019-13997-3

Charpentier, J.C., and P.D. King. 2021. Mechanisms and functions of endocytosis in T cells. *Cell Commun. Signal.* 19:92. https://doi.org/10.1186/s12964-021-00766-3

Delgoffe, G.M., C. Xu, C.L. Mackall, M.R. Green, S. Gottschalk, D.E. Speiser, D. Zehn, and P.A. Beavis. 2021. The role of exhaustion in CAR T cell therapy. *Cancer Cell*. 39:885–888. https://doi.org/10.1016/j.ccell.2021.06.012

Doan, A.E., K.P. Mueller, A.Y. Chen, G.T. Rouin, Y.S. Chen, B. Daniel, J. Lattin, M. Markovska, B. Mozarsky, J. Arias-Umana, et al. 2024. FOXO1 is a master regulator of memory programming in CAR T cells. *Nature*. 629:211–218. https://doi.org/10.1038/s41586-024-07300-8

Finetti, F., L. Patrussi, G. Masi, A. Onnis, D. Galgano, O.M. Lucherini, G.J. Pazour, and C.T. Baldari. 2014. Specific recycling receptors are targeted to the immune synapse by the intraflagellar transport system. *J. Cell Sci.* 127:1924–1937. https://doi.org/10.1242/jcs.139337

Garfall, A.L., A.D. Cohen, S.P. Susanibar-Adaniya, W.T. Hwang, D.T. Vogl, A.J. Waxman, S.F. Lacey, V.E. Gonzalez, J.A. Fraietta, M. Gupta, et al. 2023. Anti-BCMA/CD19 CAR T cells with early immunomodulatory maintenance for multiple myeloma responding to initial or later-line therapy. *Blood Cancer Discov.* 4:118–133. https://doi.org/10.1158/2643-3230.BCD-22-0074

Good, C.R., M.A. Aznar, S. Kuramitsu, P. Samareh, S. Agarwal, G. Donahue, K. Ishiyama, N. Wellhausen, A.K. Rennels, Y. Ma, et al. 2021. An NK-like CAR T cell transition in CAR T cell dysfunction. *Cell*. 184:6081–6100.e26. https://doi.org/10.1016/j.cell.2021.11.016

Grbovic, O.M., P.M. Mathews, Y. Jiang, S.D. Schmidt, R. Dinakar, N.B. Summers-Terio, B.P. Ceresa, R.A. Nixon, and A.M. Cataldo. 2003. Rab5-stimulated up-regulation of the endocytic pathway increases intracellular beta-cleaved amyloid precursor protein carboxyl-terminal fragment levels and Abeta production. *J. Biol. Chem.* 278:31261–31268. https://doi.org/10.1074/jbc.M304122200

Hamieh, M., A. Dobrin, A. Cabriolu, S.J.C. van der Stegen, T. Giavridis, J. Mansilla-Soto, J. Eyquem, Z.G. Zhao, B.M. Whitlock, M.M. Miele, et al. 2019. CAR T cell trogocytosis and cooperative killing regulate tumour antigen escape. *Nature*. 568:112–116. https://doi.org/10.1038/s41586-019-1054-1

Hayes, S., A. Chawla, and S. Corvera. 2002. TGF beta receptor internalization into EEA1-enriched early endosomes: Role in signaling to Smad2. *J. Cell Biol.* 158:1239–1249. https://doi.org/10.1083/jcb.200204088

Homma, Y., S. Hiragi, and M. Fukuda. 2021. Rab family of small GTPases: An updated view on their regulation and functions. *Febs J.* 288:36–55. https://doi.org/10.1111/febs.15453

Huang, J., M. Brameshuber, X. Zeng, J. Xie, Q.J. Li, Y.H. Chien, S. Valitutti, and M.M. Davis. 2013. A single peptide-major histocompatibility complex ligand triggers digital cytokine secretion in CD4(+) T cells. *Immunity*. 39:846–857. https://doi.org/10.1016/j.immuni.2013.08.036

Huang, J.F., Y. Yang, H. Sepulveda, W.X. Shi, I. Hwang, P.A. Peterson, M.R. Jackson, J. Sprent, and Z.L. Cai. 1999. TCR-mediated internalization of peptide-MHC complexes acquired by T cells. *Science*. 286:952–954. https://doi.org/10.1126/science.286.5441.952

Hwang, I., J.F. Huang, H. Kishimoto, A. Brunmark, P.A. Peterson, M.R. Jackson, C.D. Surh, Z. Cai, and J. Sprent. 2000. T cells can use either T cell receptor or CD28 receptors to absorb and internalize cell surface molecules derived from antigen-presenting cells. *J. Exp. Med.* 191:1137–1148. https://doi.org/10.1084/jem.191.7.1137

June, C.H., R.S. O'Connor, O.U. Kawalekar, S. Ghassemi, and M.C. Milone. 2018. CAR T cell immunotherapy for human cancer. *Science*. 359:1361–1365. https://doi.org/10.1126/science.aar6711

Kagoya, Y., S. Tanaka, T. Guo, M. Anczurowski, C.H. Wang, K. Saso, M.O. Butler, M.D. Minden, and N. Hirano. 2018. A novel chimeric antigen receptor containing a JAK-STAT signaling domain mediates superior antitumor effects. *Nat. Med.* 24:352–359. https://doi.org/10.1038/nm.4478

Kim, G.B., J. Fritsche, S. Bunk, A. Mahr, F. Unverdorben, K. Tosh, H. Kong, C.R. Maldini, C. Lau, S. Srivatsa, et al. 2022. Quantitative immunopeptidomics reveals a tumor stroma-specific target for T cell therapy. *Sci. Transl. Med.* 14:eabo6135. https://doi.org/10.1126/scitranslmed.abo6135

Kim, H., K.E. Kim, E. Madan, P. Martin, R. Gogna, H.W. Rhee, and K.J. Won. 2024. Unveiling contact-mediated cellular crosstalk. *Trends Genet.* 40:868–879. https://doi.org/10.1016/j.tig.2024.05.010

Kim, J., S. Park, J. Kim, Y. Kim, H.M. Yoon, B.R. Rayhan, J. Jeong, A.L.M. Bothwell, and J.H. Shin. 2025. Trogocytosis-mediated immune evasion in the tumor microenvironment. *Exp. Mol. Med.* 57:1–12. https://doi.org/10.1038/s12276-024-01364-2

Le Borgne, R., and F. Schweisguth. 2003. Notch signaling: Endocytosis makes delta signal better. *Curr. Biol.* 13:R273–R275. https://doi.org/10.1016/s0960-9822(03)00199-4

Leibman, R.S., M.W. Richardson, C.T. Ellebrecht, C.R. Maldini, J.A. Glover, A.J. Secreto, I. Kulikovskaya, S.F. Lacey, S.R. Akkina, Y. Yi, et al. 2017. Supraphysiologic control over HIV-1 replication mediated by CD8 T cells expressing a re-engineered CD4-based chimeric antigen receptor. *PLoS Pathog.* 13:e1006613. https://doi.org/10.1371/journal.ppat.1006613

Li, W.T., S.Z. Qiu, J. Chen, S.T. Jiang, W.D. Chen, J.W. Jiang, F. Wang, W. Si, Y.L. Shu, P. Wei, et al. 2020. Chimeric antigen receptor designed to prevent ubiquitination and downregulation showed durable antitumor efficacy. *Immunity*. 53:456–470.e6. https://doi.org/10.1016/j.immuni.2020.07.011

Longatti, A., C.A. Lamb, M. Razi, S. Yoshimura, F.A. Barr, and S.A. Tooze. 2012. TBC1D14 regulates autophagosome formation via Rab11- and ULK1-positive recycling endosomes. *J. Cell Biol.* 197:659–675. https://doi.org/10.1083/jcb.201111079

Lynn, R.C., E.W. Weber, E. Sotillo, D. Gennert, P. Xu, Z. Good, H. Anbunathan, J. Lattin, R. Jones, V. Tieu, et al. 2019. c-Jun overexpression in CAR T cells induces exhaustion resistance. *Nature*. 576:293–300. https://doi.org/10.1038/s41586-019-1805-z

Malik-Chaudhry, H.K., K. Prabhakar, H.S. Ugamraj, A.A. Boudreau, B. Buelow, K. Dang, L.M. Davison, K.E. Harris, B. Jorgensen, H. Ogana, et al. 2021. TNB-486 induces potent tumor cell cytotoxicity coupled with low cytokine release in preclinical models of B-NHL. *MAbs*. 13:1890411. https://doi.org/10.1080/19420862.2021.1890411

Medvec, A.R., C. Ecker, H. Kong, E.A. Winters, J. Glover, A. Varela-Rohena, and J.L. Riley. 2018. Improved expansion and in vivo function of patient T cells by a serum-free medium. *Mol. Ther. Methods Clin. Dev.* 8:65–74. https://doi.org/10.1016/j.omtm.2017.11.001

Melenhorst, J.J., G.M. Chen, M. Wang, D.L. Porter, C. Chen, M.A. Collins, P. Gao, S. Bandyopadhyay, H. Sun, Z. Zhao, et al. 2022. Decade-long leukaemia remissions with persistence of CD4(+) CAR T cells. *Nature*. 602:503–509. https://doi.org/10.1038/s41586-021-04390-6

Milone, M.C., J.D. Fish, C. Carpenito, R.G. Carroll, G.K. Binder, D. Teachey, M. Samanta, M. Lakhal, B. Gloss, G. Danet-Desnoyers, et al. 2009. Chimeric receptors containing CD137 signal transduction domains mediate enhanced survival of T cells and increased antileukemic efficacy in vivo. *Mol. Ther.* 17:1453–1464. https://doi.org/10.1038/mt.2009.83

Moon, E.K., L.C. Wang, D.V. Dolfi, C.B. Wilson, R. Ranganathan, J. Sun, V. Kapoor, J. Scholler, E. Pure, M.C. Milone, et al. 2014. Multifactorial T-cell hypofunction that is reversible can limit the efficacy of chimeric antigen receptor-transduced human T cells in solid tumors. *Clin. Cancer Res.* 20:4262–4273. https://doi.org/10.1158/1078-0432.CCR-13-2627

Narayan, V., J.S. Barber-Rotenberg, I.Y. Jung, S.F. Lacey, A.J. Rech, M.M. Davis, W.T. Hwang, P. Lal, E.L. Carpenter, S.L. Maude, et al. 2022. PSMA-targeting TGFbeta-insensitive armored CAR T cells in metastatic castration-resistant prostate cancer: A phase 1 trial. *Nat. Med.* 28:724–734. https://doi.org/10.1038/s41591-022-01726-1

Olson, M.L., E.R.V. Mause, S.V. Radhakrishnan, J.D. Brody, A.P. Rapoport, A.L. Welm, D. Atanackovic, and T. Luetkens. 2022. Low-affinity CAR T cells exhibit reduced trogocytosis, preventing rapid antigen loss, and increasing CAR T cell expansion. *Leukemia*. 36:1943–1946. https://doi.org/10.1038/s41375-022-01585-2

Pagliano, O., R.M. Morrison, J.M. Chauvin, H. Banerjee, D. Davar, Q. Ding, T. Tanegashima, W. Gao, S.R. Chakka, R. DeBlasio, et al. 2022. Tim-3 mediates T cell trogocytosis to limit antitumor immunity. *J. Clin. Invest.* 132:e152864. https://doi.org/10.1172/JCI152864

Rafiq, S., C.S. Hackett, and R.J. Brentjens. 2020. Engineering strategies to overcome the current roadblocks in CAR T cell therapy. *Nat. Rev. Clin. Oncol.* 17:147–167. https://doi.org/10.1038/s41571-019-0297-y

Rechavi, O., I. Goldstein, and Y. Kloog. 2009. Intercellular exchange of proteins: The immune cell habit of sharing. *FEBS Lett.* 583:1792–1799. https://doi.org/10.1016/j.febslet.2009.03.014

Redpath, G.M.I., M. Ecker, N. Kapoor-Kaushik, H. Vartoukian, M. Carnell, D. Kempe, M. Biro, N. Ariotti, and J. Rossy. 2019. Flotillins promote T cell receptor sorting through a fast Rab5-Rab11 endocytic recycling axis. *Nat. Commun.* 10:4392. https://doi.org/10.1038/s41467-019-12352-w

Rossatti, P., G.M.I. Redpath, L. Ziegler, G.P.B. Samson, C.D. Clamagirand, D.F. Legler, and J. Rossy. 2022. Rapid increase in transferrin receptor recycling promotes adhesion during T cell activation. *BMC Biol.* 20:189. https://doi.org/10.1186/s12915-022-01386-0

Sara, Y., T. Virmani, F. Deak, X. Liu, and E.T. Kavalali. 2005. An isolated pool of vesicles recycles at rest and drives spontaneous neurotransmission. *Neuron*. 45:563–573. https://doi.org/10.1016/j.neuron.2004.12.056

Shin, J.H., J. Jeong, S.E. Maher, H.W. Lee, J. Lim, and A.L.M. Bothwell. 2021. Colon cancer cells acquire immune regulatory molecules from tumor-infiltrating lymphocytes by trogocytosis. *Proc. Natl. Acad. Sci. USA*. 118: e2110241118. https://doi.org/10.1073/pnas.2110241118

Shukla, D., K. Gabunia, S.E. McGettigan, P.R. Patel, S. Christensen, T.J. Fan, D. Song, Y. Luo, Y. Wang, H. Wang, et al. 2025a. CAR binders affect CAR T-cell tonic signaling, durability, and sensitivity to target. *Cancer Immunol. Res.* 13:867–880. https://doi.org/10.1158/2326-6066.CIR-24-1347

Shukla, D., S. Manne, S. Jiang, M. Ruella, E.J. Wherry, and J.L. Riley. 2025b. Optimal pairing of binder and co-stimulatory domains improves dual CART cell efficacy. *Mol. Ther.* 33:5556–5571. https://doi.org/10.1016/j.ymthe.2025.08.002

Shum, T., B. Omer, H. Tashiro, R. Kruse, D. Wagner, K. Parikh, Z.Z. Yi, T. Sauer, R. Parihar, L. Metelitsa, et al. 2017. Constitutive signaling from an engineered IL-7 receptor promotes durable tumor elimination by tumor redirected T-cells. *Mol. Ther.* 25:250. https://doi.org/10.1158/2159-8290.CD-17-0538

Soreng, K., T.P. Neufeld, and A. Simonsen. 2018. Membrane trafficking in autophagy. *Int. Rev. Cell Mol. Biol.* 336:1–92. https://doi.org/10.1016/bs.ircmb.2017.07.001

Stinchcombe, J.C., Y. Asano, C.J.G. Kaufman, K. Bohlig, C.J. Peddie, L.M. Collinson, A. Nadler, and G.M. Griffiths. 2023. Ectocytosis renders T cell receptor signaling self-limiting at the immune synapse. *Science*. 380: 818–823. https://doi.org/10.1126/science.abp8933

Stopfer, L.E., J.M. Mesfin, B.A. Joughin, D.A. Lauffenburger, and F.M. White. 2020. Multiplexed relative and absolute quantitative immunopeptidomics reveals MHC I repertoire alterations induced by CDK4/6 inhibition. *Nat. Commun.* 11:2760. https://doi.org/10.1038/s41467-020-16588-9

Sun, F., Y. Cheng, V. Wanchai, W. Guo, D. Mery, H. Xu, D. Gai, E. Siegel, C. Bailey, C. Ashby, et al. 2024. Bispecific BCMA/CD24 CAR-T cells control multiple myeloma growth. *Nat. Commun.* 15:615. https://doi.org/10.1038/s41467-024-44873-4

Tekguc, M., J.B. Wing, M. Osaki, J. Long, and S. Sakaguchi. 2021. Treg-expressed CTLA-4 depletes CD80/CD86 by trogocytosis, releasing free PD-L1 on antigen-presenting cells. *Proc. Natl. Acad. Sci. USA*. 118: e2023739118. https://doi.org/10.1073/pnas.2023739118

Walker, A.J., R.G. Majzner, L. Zhang, K. Wanhainen, A.H. Long, S.M. Nguyen, P. Lopomo, M. Vigny, T.J. Fry, R.J. Orentas, and C.L. Mackall. 2017. Tumor antigen and receptor densities regulate efficacy of a chimeric antigen receptor targeting anaplastic lymphoma kinase. *Mol. Ther.* 25: 2189–2201. https://doi.org/10.1016/j.ymthe.2017.06.008

Wang, X., J. Cheng, L. Shen, M. Chen, K. Sun, J. Li, M. Li, C. Ma, and L. Wei. 2024. Rab5c promotes RSV and ADV replication by autophagy in respiratory epithelial cells. *Virus Res.* 341:199324. https://doi.org/10.1016/j.virusres.2024.199324

Ward, E.S., C. Martinez, C. Vaccaro, J. Zhou, Q. Tang, and R.J. Ober. 2005. From sorting endosomes to exocytosis: Association of Rab4 and Rab11 GTPases with the Fc receptor, FcRn, during recycling. *Mol. Biol. Cell*. 16: 2028–2038. https://doi.org/10.1091/mbc.e04-08-0735

Wei, F., S. Zhong, Z. Ma, H. Kong, A. Medvec, R. Ahmed, G.J. Freeman, M. Krogsgaard, and J.L. Riley. 2013. Strength of PD-1 signaling differentially affects T-cell effector functions. *Proc. Natl. Acad. Sci. USA*. 110: E2480–E2489. https://doi.org/10.1073/pnas.1305394110

Xie, S., J. Long, R. Wang, R. Xiang, H. Xian, Y. Wang, W. Dou, W. Zhang, D. Li, T. Kang, et al. 2025. Improved CAR internalization and recycling through transmembrane domain optimization reduces CAR-T cytokine release and exhaustion. *Front. Immunol.* 16:1531344. https://doi.org/10.3389/fimmu.2025.1531344

Xu, X., H. Chen, Z. Ren, X. Xu, W. Wu, H. Yang, J. Wang, Y. Zhang, Q. Zhou, H. Li, et al. 2024. Phase separation of chimeric antigen receptor promotes immunological synapse maturation and persistent cytotoxicity. *Immunity*. 57:2755–2771.e8. https://doi.org/10.1016/j.immuni.2024.11.005

Yuan, W., and C. Song. 2020. The emerging role of Rab5 in membrane receptor trafficking and signaling pathways. *Biochem. Res. Int.* 2020: 4186308. https://doi.org/10.1155/2020/4186308

Zerial, M., and H. McBride. 2001. Rab proteins as membrane organizers. *Nat. Rev. Mol. Cell Biol.* 2:107–117. https://doi.org/10.1038/35052055

Zhai, Y., Y. Du, G. Li, M. Yu, H. Hu, C. Pan, D. Wang, Z. Shi, X. Yan, X. Li, et al. 2023. Trogocytosis of CAR molecule regulates CAR-T cell dysfunction and tumor antigen escape. *Signal. Transduct. Target Ther.* 8:457. https://doi.org/10.1038/s41392-023-01708-w

Zhen, Y., and H. Stenmark. 2015. Cellular functions of Rab GTPases at a glance. *J. Cell Sci.* 128:3171–3176. https://doi.org/10.1242/jcs.166074

Zhou, X., H. Cao, S.Y. Fang, R.D. Chow, K. Tang, M. Majety, M. Bai, M.B. Dong, P.A. Renauer, X. Shang, et al. 2023. CTLA-4 tail fusion enhances CAR-T antitumor immunity. *Nat. Immunol.* 24:1499–1510. https://doi.org/10.1038/s41590-023-01571-5

JEM

Supplemental material

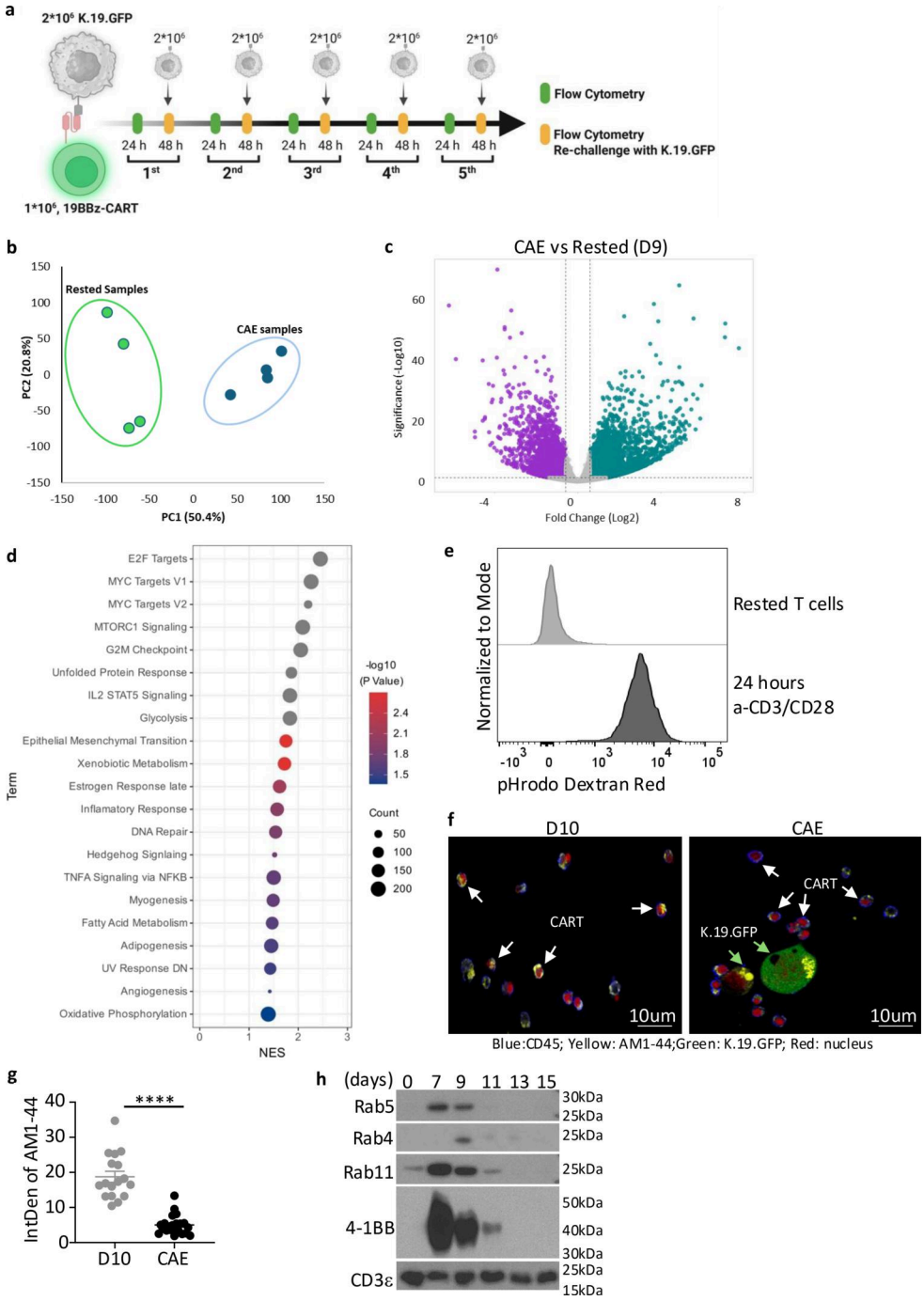

Figure S1. **Continuous tumor interactions lead to downregulation of endocytic activity in CARTs. (a)** Schematic of CAE assay. **(b)** Principal component analysis (PCA) of bulk RNA-seq data from 19BBz-tEGFR CARTs cultured in the presence (CAE samples) or absence (rested samples, D9) of K.19.GFP tumor cells. Each dot represents an individual donor sample. Separation along PC1 and PC2 reflect transcriptomic differences driven by tumor engagement. **(c)** Volcano plots of bulk RNA-seq data displaying gene expression changes in 19BBz-tEGFR CARTs cultured in the presence or absence of K.19.GFP tumor cells. Significantly (P value <0.05) upregulated genes (>twofold), downregulated genes (<-twofold), and unchanged genes are highlighted in green, purple, and grey, respectively. **(d)** Normalized enrichment score (NES) for biological pathways obtained post GO analysis, comparing 19BBz-tEGFR CARTs cultured with or without K.19.GFP tumor cells. Data in b–d are representative of four samples from different donors. **(e)** Endocytic activity of rested T cells or T cells activated with anti-CD3/CD28 beads for 24 h was measured by uptake of pHrodo Red dextran using flow cytometry. Data are representative of three independent experiments with samples from independent healthy donors. **(f)** Endocytic activity of 19BBz-tEGFR CARTs was assessed by AM1-44 uptake in the absence or presence of K.19.GFP and visualized by confocal microscopy. GFP (green), endogenous CD45 (blue), nuclei (red), and AM1-44 (yellow) are shown. **(g)** Integrated density (IntDen) of AM1-44 dye in T cells shown in f was quantified using ImageJ. Data in f and g are representative of two independent experiments with samples from independent healthy donors. **(h)** Western blot analysis of Rab protein expression in CARTs before they were treated by tumor cells. Primary human T cells were activated on day 1, which induced Rab protein expression. Following anti-CD3/CD28 beads removal on day 3, Rab protein levels were downregulated. Data are representative of three independent experiments with samples from independent healthy donors. Error bars show mean ± SEM. Statistical comparisons were made using unpaired *t* tests. ****P < 0.0001. Source data are available for this figure: SourceData FS1.

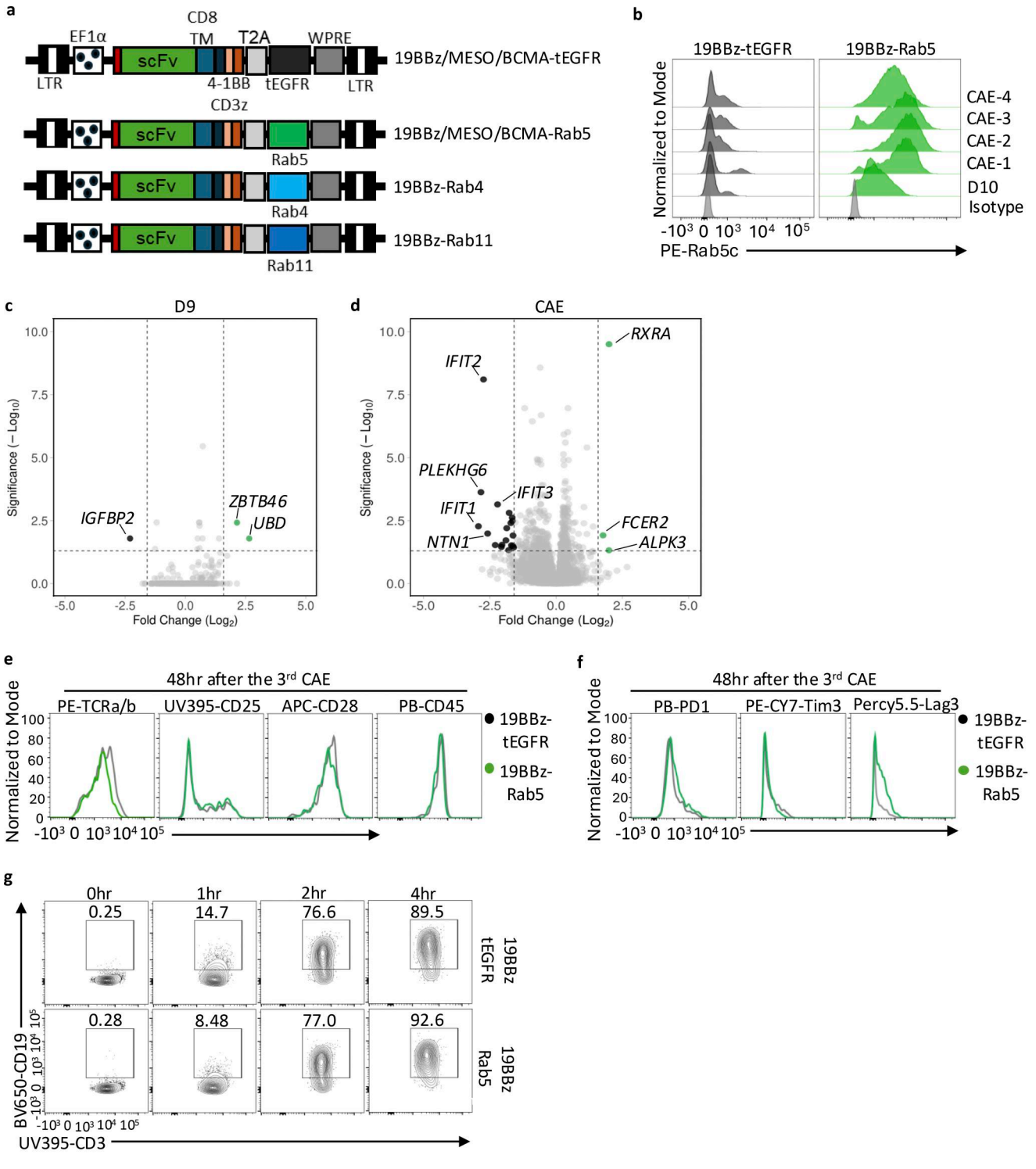

Figure S2. **Rab5 does not affect CART activation and short-term antigen capture. (a)** Schematic representation of Rab protein expression 19BBz, MESOBBz, and BCMABBz CAR constructs. These constructs are the same with substituted scFv regions targeting CD19, mesothelin, and BCMA antigens, respectively. **(b)** Intracellular flow cytometry staining of Rab5 expression in both control and Rab5-CARTs during CAE assay. Data are representative of two independent experiments with samples from independent healthy donors. **(c and d)** Volcano plots of differential gene expression in control and Rab5 CARTs, from bulk RNA-seq. Significantly (P value <0.05) upregulated genes (>twofold), downregulated genes (≤twofold), and unchanged genes are highlighted in green, black, and grey, respectively. Data are representative of four samples from different donors. **(e and f)** Expression levels of the indicated surface markers (e) and the expression of T cell exhaustion markers (f) was comparable between 19BBz-tEGFR and -Rab5 CARTs. Data are representative of three independent experiments with samples from independent healthy donors. **(g)** Representative flow cytometry of $CD3^+CD19^+$ CARTs cultured with K.19.GFP cells. 19BBz-tEGFR or -Rab5 CARTs displayed comparable CD19 trogocytosis after short-term incubation at indicated time points. Data are representative of two independent experiments with samples from independent healthy donors.

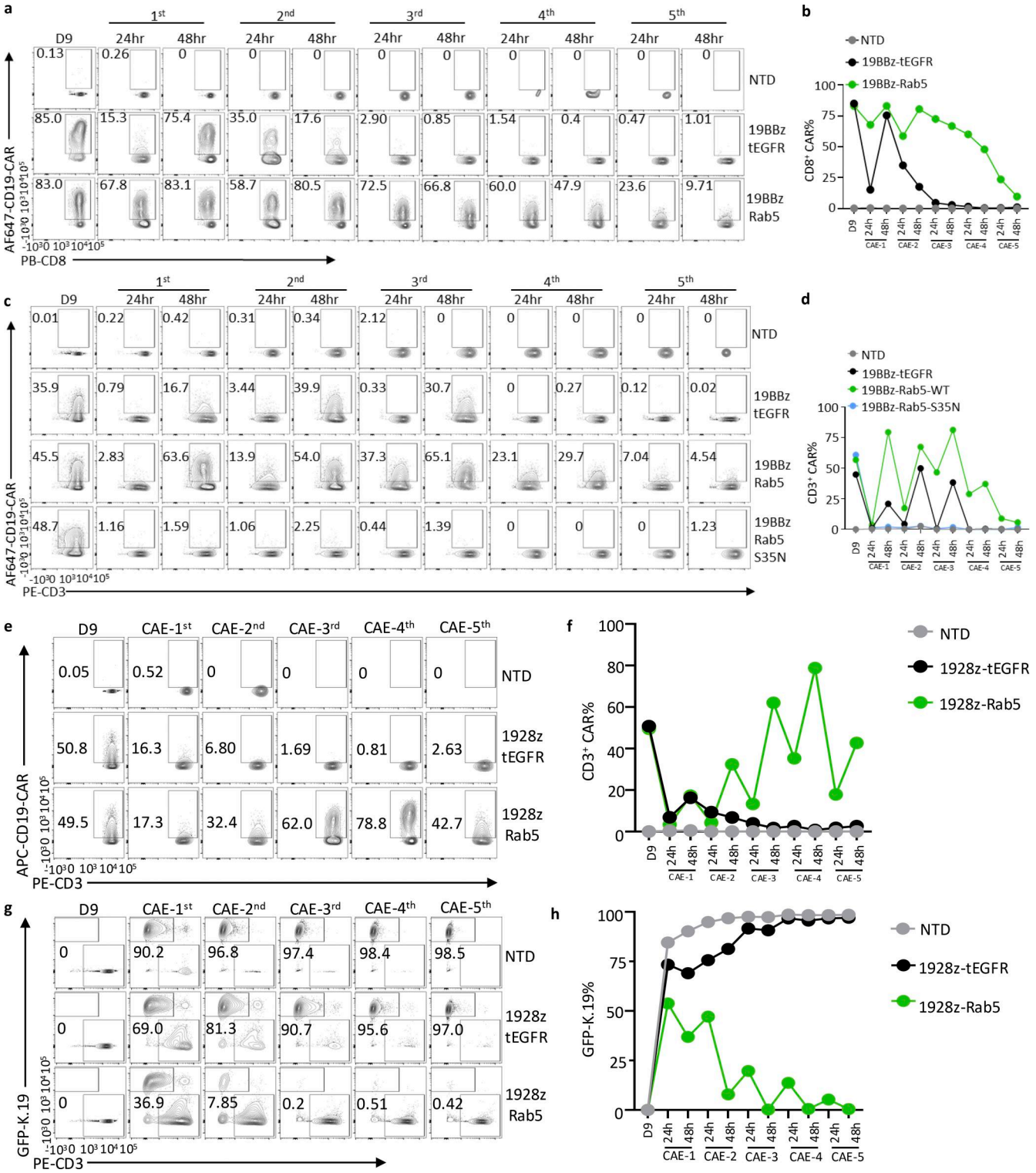

Figure S3. **Rab5 expression maintains surface CARs on CARTs. (a and b)** The ability of 19BBz-tEGFR and 19BBz-Rab5 CD8⁺ CARTs to bind CD19 protein shown by representative flow cytometry plots (a) and summary data (b) during the CAE assay. **(c and d)** The ability of 19BBz-tEGFR, 19BBz-Rab5, or 19BBz-Rab5-S35N CARTs to bind CD19 protein, shown by representative flow cytometry plots (c) and summary data (d) during the CAE assay. **(e and f)** The ability of T cells transduced with 1928z-tEGFR or 1928z-Rab5 vectors to bind CD19 protein was measured during the CAE assay by flow cytometry. **(g and h)** The ability of T cells transduced with 1928z-tEGFR or 1928z-Rab5 vectors to control tumor cells was measured during the CAE assay by flow cytometry. Data in a–h are representative of three independent experiments with samples from independent healthy donors.

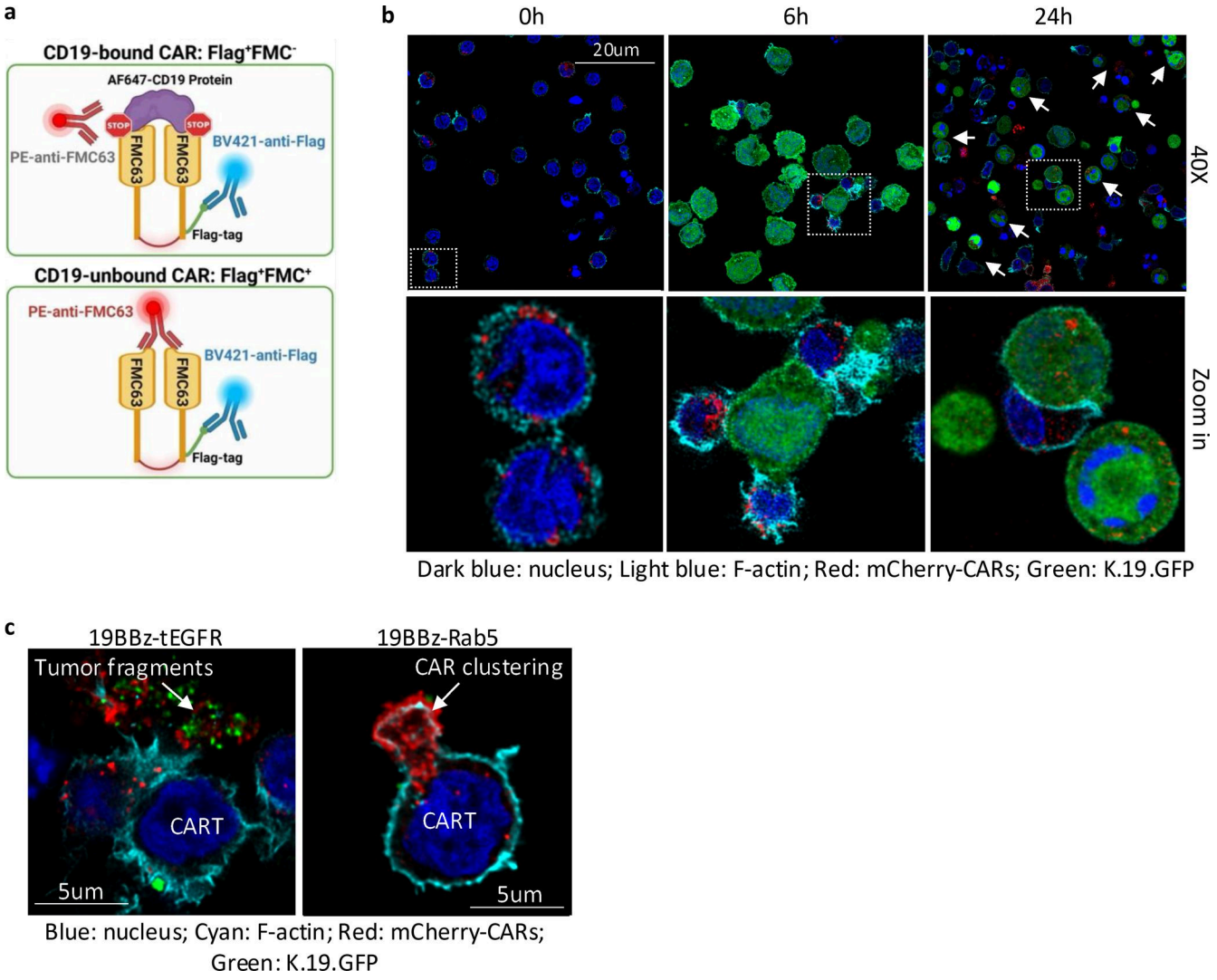

Figure S4. **Rab5 expression inhibits CAR trogocytosis into tumor cells. (a)** Staining strategy for detecting unengaged CARs using FLAG-tagged CARTs. FLAG-tagged 19BBz CARTs were incubated with CD19 protein at 37°C for 1 h to allow formation of CD19–CAR complexes, followed by endocytosis and potential dissociation. To track if CARs were bound to CD19 protein or not, cells were incubated with anti-FMC63 antibody, which recognizes the scFv domain of 19BBz CARs, at 37°C for indicate time point. CARs that were released from CD19 were identified as double-positive for both anti-FLAG and anti-FMC63 staining by flow cytometry. **(b)** High-resolution confocal imaging of the cellular localization of mCherry-CARs (red) between CARTs and GFP-expressing tumor cells (green) during the indicated time of engagement. T cell surface (F-actin, cyan) and nuclei (dark blue) are shown. The arrow indicates tumor cells exhibiting cytosolic uptake of mCherry-fused CARs. Data are representative of three independent experiments with samples from independent healthy donors. **(c)** High-content microscopy showing the spatial distribution of antigen and CARs in control and Rab5-CARTs during the third-round CAE assay. Control and Rab5-CARTs expressing mCherry-CARs (red) were co-cultured with K.19.GFP cells (green), then fixed, and stained with Hoechst 33342 (blue) to label nuclei and F-actin (cyan) to delineate the cell membrane. Data are representative of two independent experiments with samples from independent healthy donors.

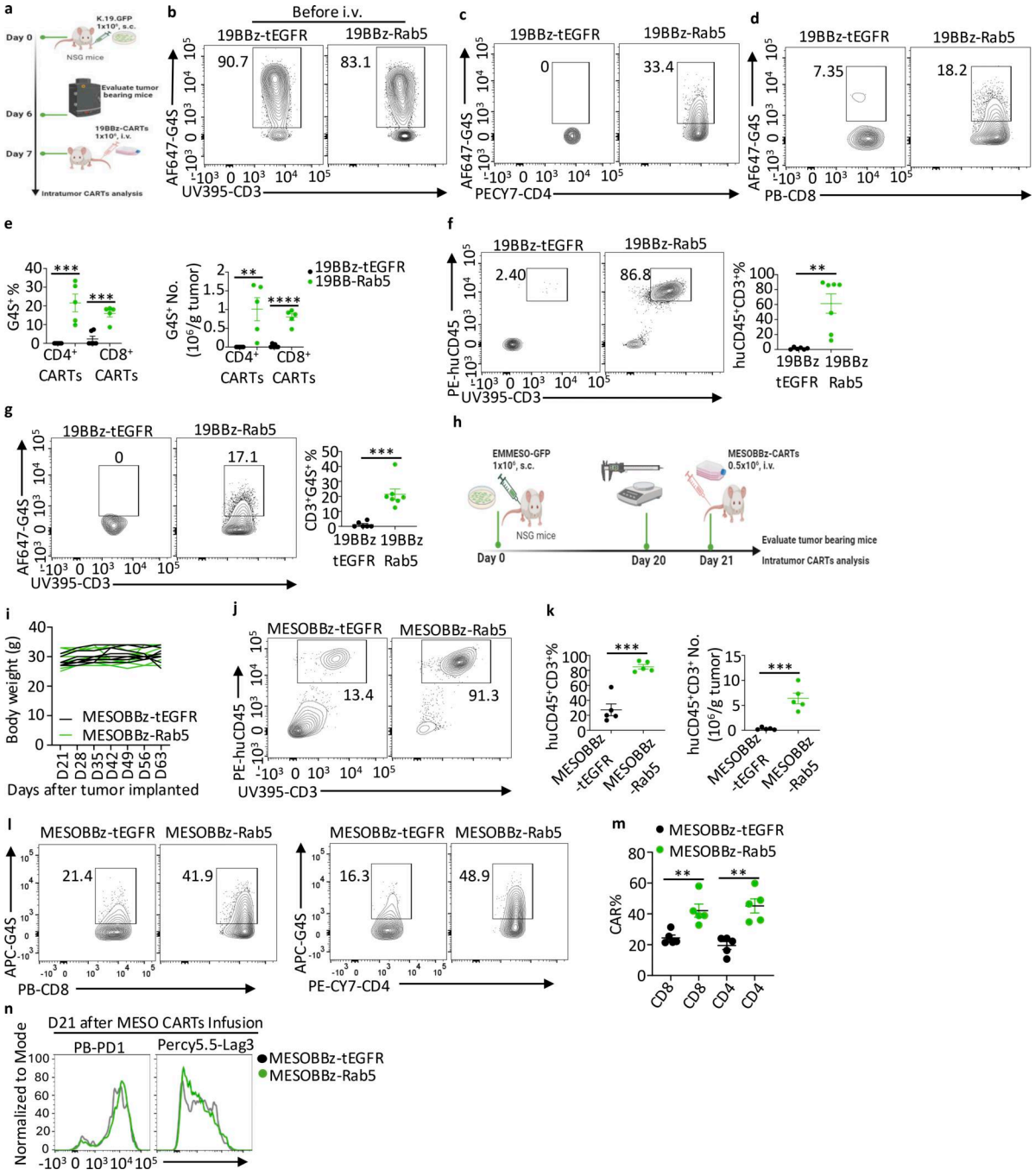

Figure S5. **Rab5 expression augments the ability of CARTs to control solid tumors. (a)** Experimental design of *in vivo* tumor challenge mouse model. 1 × 10^6 K.19.GFP cells mixed with Matrigel were s.c. injected to NSG mice on day 0. Tumors were imaged 6 days later, followed by tail i.v. injection with 1 × 10^6 19BBz CARTs on day 7. **(b)** Surface CAR expression level between 19BBz-tEGFR and -Rab5 CARTs before infusion. Data are representative of five independent experiments with samples from independent healthy donors. **(c–e)** Surface CAR expression and absolute CARTs number of $CD4^+$ (c and e), and $CD8^+$ CARTs (d and e) isolated from tumors after 14 days CARTs infusion. Data are representative of two independent experiments, *n* = 5–7 mice for each group. **(f)** Peripheral blood CART expansion was measured 14 days after infusion of 19BBz-tEGFR or -Rab5 CARTs into K.19.GFP tumor-bearing mice. Data are representative of two independent experiments, *n* = 5–7 mice for each group. **(g)** CAR expression in CARTs from samples in f 14 days after infusion. Data are representative of two independent experiments, *n* = 5–7 mice for each group. **(h)** Schematic of mesothelin tumor mouse model. 1 × 10^6 EMMESO-GFP or AsPC-1 cells were s.c. injected to NSG mice. Tumor size reached around 150 mm^3 after 20 days, 0.5 × 10^6 NTD, MESOBBz-tEGFR or MESOBBz-Rab5 CARTs were infused i.v. on day 21. **(i)** Body weight of individual EMMESO-tumor–bearing mice was monitored weekly from the day of MESOBBz CART infusion. Data are representative of three independent experiments, *n* = 5–11 mice for each group. **(j and k)** Expansion of tumor-infiltrating MESOBBz CARTs was detected after 21 days infusion using anti-huCD45 and anti-huCD3 antibodies. Data are representative of two independent experiments, *n* = 5 mice for each group. **(l and m)** CAR surface expression in both $CD4^+$ and $CD8^+$ intratumoral CARTs after 21 days infusion was assessed by flow cytometry (l), and representative data for the percentage of intratumoral CARTs are shown (m). Data are representative of two independent experiments, *n* = 5 mice for each group. **(n)** Exhaustion markers on tumor infiltrating MESOBBz-tEGFR or -Rab5 CARTs were determined 21 days after infusion. Data are representative of two independent experiments, *n* = 5 mice for each group. Error bar show mean± SEM. Statistical comparisons were made using unpaired *t* tests. **P < 0.01, ***P < 0.001, and ****P < 0.0001.